A THEORETICAL ANALYSIS OF JET DEFLECTION FROM PLANE AND AXISYMMETRIC CURVED OBSTACLES

Gerardo Hiriart Le-Bert

NAVAL POSTGRADUATE SCHOOL
Monterey, California

THESIS

A THEORETICAL ANALYSIS OF JET DEFLECTION FROM PLANE AND AXISYMMETRIC CURVED OBSTACLES

by

Gerardo HIRIART Le-Bert

Thesis Advisor: T. Sarpkaya

December 1973

Approved for public release; distribution unlimited.

A Theoretical Analysis of Jet Deflection From Plane and Axisymmetric Curved Obstacles

by

Gerardo HIRIART Le-Bert
Teniente 1°, Armada de Chile
M.S. and M.E., Naval Postgraduate School, 1970

Submitted in partial fulfillment of the
requirements for the degree of

DOCTOR OF PHILOSOPHY

from the
NAVAL POSTGRADUATE SCHOOL
December 1973

ABSTRACT

A class of analytical and numerical solutions to the problem of inviscid-jet deflection from plane and axisymmetric concave surfaces are presented. The methods of solution for the two-dimensional cases included a novel method developed in the present investigation, as well as those due to Levi-Civita and Riemann and Hilbert. These methods have provided indirect solutions for the shape of the curved solid boundary in terms of a given jet-departure and jet-deflection angle. The axisymmetric cases, namely, the deflection of axisymmetric jets from hemispherical thrust reversers are solved directly through the use of the finite element method and a novel iteration scheme. The real-fluid effects on the jet deflection are estimated by comparing the results with those obtained experimentally.

The analytical and numerical methods developed or used herein are sufficiently general to yield direct and indirect solutions for more general nozzle and curved-reverser combinations of special interest to thrust reversal on aircraft engines.

TABLE OF CONTENTS

LIST OF FIGURES

NOMENCLATURE

A	area of the meridional plane
A^e	area of a triangular element e
A_i	area of a subtriangle in a triangular element
a	a parameter
a_k	$x_j - x_i$
a_n	coefficients of a series
B_i^e	load matrix for element e
b	a parameter
b_k	$r_i - r_j$
C_T	thrust coefficient
ΔC_T	error in C_T
DELV	incremental correction to the free surface
d	jet thickness
dA	elemental area
e	denotes an element
FAC	a multiplier
FACU	a multiplier
FACL	a multiplier
f	a parameter
$f(t)$	shape function in Riemann-Hilbert method
$H(t)$	homogeneous solution of the Riemann problem
$h(\sigma)$	function of σ represented by a Fourier sine series
$I(\phi)$	functional of velocity potential ϕ
$I^e(\phi)$	functional I for an element e
Im[ ]	imaginary part of [ ]

i	$\sqrt{-1}$
K_{ij}^{e}	elements of the stifness matrix for element e
k	a parameter
l_1, l_2, l_3	side lengths of a triangle
M	number of triangular elements
M_o	a complex constant
N	number of terms in a series
N_o	a complex constant
P	pressure
P_o	pressure at the entrance of the nozzle
$Q(t)$	function of t in the Riemann-Hilbert method
q	magnitude of velocity
R_o	radius of the lip of the bucket
$R_e[\ ]$	real part of [ ]
r	radial coordinate, also modulus of ζ
r_o	radius of the nozzle
r_E, r_F, r_G	radial coordinates of the points E, F and G
r_1, r_2, r_3	radial coordinates of corner nodal points 1, 2 and 3 in a triangular element
S	a complex variable
S_{ij}	an array related to the geometry of each element
s	separation between the nozzle and the bucket lip
T	thrust
$T_i^e, \tilde{T}_i^e$	arrays expressing the geometrical characteristics of an element
t	a variable
u, v	horizontal and radial components of velocity
u^e, v^e	velocities in an element e

V	magnitude of velocity
V_o	velocity at the entrance of the nozzle
V_c	velocity at the point C
V_j	final freestream velocity, (here $V_j = 1$)
V_s	velocity at a point over the assumed free streamline
VC	denotes V_c
VØ	denotes V_o
VS	denotes V_s
W	complex potential function
x,y	cartesian coordinate
x_q,y_q	coordinates of the point Q
z	a complex variable
α_p,α_q	exterior angles of a polygon at P and Q
β	deflection angle
ζ	a complex variable
ζ_i	area coordinates
η	a dummy variable
η_R	reverse-thrust efficiency
θ	direction of the velocity vector
λ	a constant
ρ	density of fluid
σ	argument of ζ
ϕ	velocity potential
ϕ^e	velocity potential in an element e
$(\frac{\partial\phi}{\partial n})^a$	specified normal derivative
χ_i	array of area coordinates

ψ	stream function
Ω	a complex variable
ω	a complex function of the velocity vector

ACKNOWLEDGEMENTS

The author owes a particular debt of gratitude to Professor T. Sarpkaya for his insight in idendifying this problem and for his invaluable help, advice, and guidance throughout the course of the investigation.

Special thanks are due my wife and children for their loving companionship, understanding, and encouragement. Finally, I wish to thank the Chilean Navy for making this study possible.

I. INTRODUCTION

The prediction of the deflection of finite jets by segmental or curved deflectors is a matter of importance in the design of target-type thrust reversers on jet-aircraft engines, of flip-buckets on spillways, of Pelton wheels, etc. In general, the deflection of a free jet by a solid boundary is well suited to potential-flow analysis because of the dominance of inertia and pressure intensity in the establishment of the flow pattern. The design of impulse machinery, thrust reversers, etc. utilizing this momentum change could be facilitated greatly if the idealized geometry of the system under potential flow conditions were known because such conditions represent asymptotic values which are approached as the effects of secondary variables such as entrainment, boundary layer, compressibility, jet attachment to adjacent surfaces, etc., are decreased. With such information available, refinements of design could be based upon a secure knowledge of the fundamentals, and many rules of thumb could be replaced with precise quantitative data. Specifically, if the total angle through which the jet is deflected is determined for conditions of both partial and complete interception by the boundary, then the principle of impulse and momentum can be used to compute forces or other dynamic characteristics of the system.

The problems discussed herein fall in the general category of finite or infinite, two-dimensional or three-dimensional,

viscous or inviscid, and compressible or incompressible flow past bodies of arbitrary shape. In fact, in its broadest sense, they constitute the most fundamental and also most complex problems of fluid dynamics. Our inability to determine the separation points, or lines, on a body and to establish a link between the separation and the unsteady fluid motion in the wake of the body gave rise to numerous exact and approximate methods of analysis. Most of these analyses rely in part or whole on the experimentally observed characteristics of flow to determine the magnitude of the disposable parameters introduced into the analysis. Suffice it to say that future efforts will continue to be based upon partly a secure knowledge of the fundamentals of fluid mechanics and partly on experimental facts.

Evidently, the introduction of simplifying assumptions such as inviscid, incompressible fluids, the use of bodies with a salient edge at which the separation point is fixed and finally the restriction of the analysis to either two-dimensional or axisymmetric flows enable one to obtain solutions which are often of practical significance and in conformity with the experimental observations.

The present work deals with inviscid, incompressible flows of finite extent impinging upon two-dimensional or axisymmetric bodies with sharp edges, and makes use of all the available exact or approximate methods of analysis in arriving at novel solutions towards the prediction of the characteristics of deflected jets.

A closer look at both the problem at hand and the methods available requires the further specification of the geometrical configurations of both the nozzle from which the jet is emerging and the body upon which the jet is impinging. The classical theory of jet deflection deals essentially with nozzles and bodies composed of straight segments. This is primarily because the successive transformations used in the analysis lead to relatively integrable equations for the segmental boundaries and to exceedingly complex integral equations in the case of curved boundaries. Furthermore, the fact that there cannot be a corresponding complex-function theory for three-dimensional space, the limitations of our understanding of the characteristics of axisymmetric or, in general, three-dimensional jet-deflection problems becomes quite clear.

In order to bring into closer focus the results of the past efforts as well as the limitations of the existing methods, we will, in the foregoing, describe briefly the suggestions made concerning the "rounding of the corners" of solid boundaries, describe the essential features of the problems encountered through the use of a specific example, and then discuss the history of the two-dimensional jet deflection problem. The comments concerning the previous work on axisymmetric jet deflection will be reserved for Section III where such cases are studied through the use of the finite element method.

A. A BRIEF REVIEW OF SEGMENTAL JET DEFLECTORS IN TWO-DIMENSIONAL FLOWS

The two-dimensional counterpart of the jet-deflection problem has been treated by several investigators through the use of the powerful analytic-function theory and successive conformal transformations. Sarpkaya [1] solved the U-shaped, two-segment, deflector problem where the turning angle between the segments is limited to 90 degrees. Tinney et al. [2] extended this analysis to the case where the turning angle between the symmetrically situated segments is greater than 90 degrees. Later, Chang and Conley [3] presented an analysis for a bucket composed of a series of segments of arbitrary number, length, and angles; however, the basic as well as practical problem of the direct analysis of jet deflection by curved buckets remains unsolved primarily because of the mathematical difficulties encountered. It is partly for the purpose of illustrating these difficulties and partly for the purpose of familiarizing the reader with the fundamental concepts and the analytical transformations that the basic steps in the analysis of the deflection of a two-dimensional jet from a U-shaped segmental deflector will be discussed.

The flow in the physical z-plane (see Fig. 1) may be transformed into a hodograph-plane through the use of

$$\zeta = -u + iv = -qe^{-i\theta} = \frac{dW}{dz} \tag{1}$$

The flow in the hodograph plane may be transformed by means

(a) z-plane

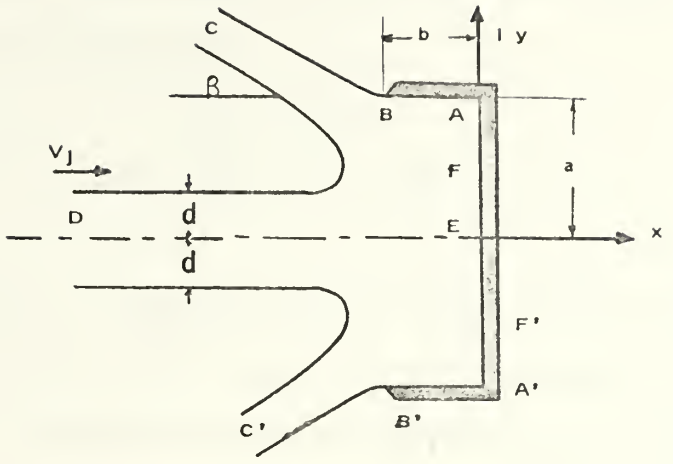

(b) ζ-plane

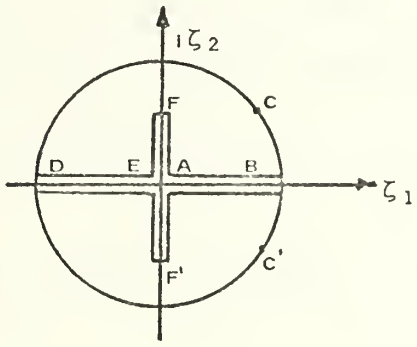

(c) Ω-plane

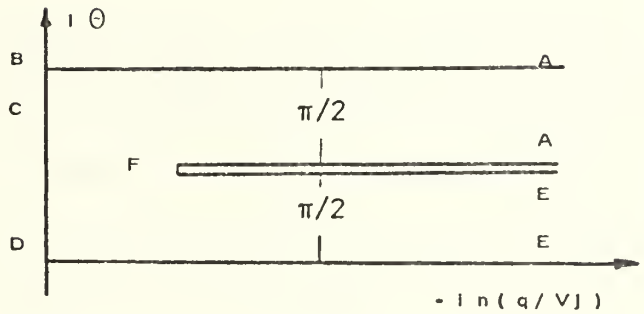

(d) t-plane

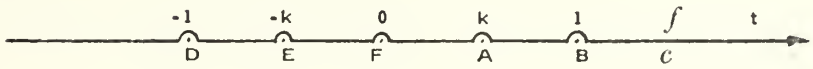

Figure 1 Transformation planes for the U-shaped bucket

of Planck's logarithmic transformation into an Ω-plane where Ω is defined by,

$$\Omega = \ln\left(-\frac{V_j}{\zeta}\right) = -\ln\frac{q}{V_j} + i\theta \qquad (2)$$

The Ω-plane is composed of straight lines. The horizontal lines represent the solid boundaries and the vertical lines the free surfaces. Such a polygon may be transformed (e.g. see Milne-Tomson [4]) through the use of the Schwarz-Christoffel transformation onto either the upper or the lower half of a t-plane by writing

$$\Omega = M_o \int \frac{dt}{(t-t_1)^{\alpha_1/\pi}(t-t_2)^{\alpha_2/\pi}\ldots} + N_o \qquad (3)$$

Three of the t values in the t-plane may be chosen arbitrarily in accordance with the Schwarz-Christoffel transformation and the rest must be assigned unknown parameters. Accordingly, the points E, A, C are assigned the values -k, k and f respectively. Then, Eq. (3) becomes

$$\Omega = M_o \int \frac{t\,dt}{(t^2-k^2)\sqrt{t^2-1}} + N_o \qquad (4)$$

After integration and evaluation of the constants M_o and N_o, one obtains

$$\Omega = \ln\frac{\sqrt{1-k^2}+\sqrt{1-t^2}}{\sqrt{t^2-k^2}} \quad \text{for } t \geq 1 \text{ and } t \leq -k \qquad (5)$$

and

$$\Omega = \ln \frac{\sqrt{1-k^2} + \sqrt{1-t^2}}{-\sqrt{t^2-k^2}} \quad \text{for } -k \leq t \leq 1 \qquad (6)$$

The potential function W in the upper half of the t-plane may be written in terms of the sources and sinks representing the flow. Noting that there is a source at D and a sink at C and that only the upper half of the t-plane is used, one has

$$W = \frac{V_j d}{\pi} [\ln (t-f) - \ln (t+1)] \qquad (7)$$

From this relationship and the definition of ζ in Eq. (1) and Ω in Eq. (2) one obtains the final expression that relates the z-plane to the t-plane,

$$\frac{z}{d} = \int \frac{\sqrt{1-t^2} + \sqrt{1-k^2}}{\sqrt{k^2-t^2}} \left[\frac{1}{t-f} - \frac{1}{t+1}\right] dt \qquad (8)$$

Since the purpose of this section was only to show the general procedure used for this type of transformations, the results of the integration are not shown here. The details are given by Sarpkaya [1].

It is apparent from the foregoing that whenever the solid boundaries in the physical plane (see Fig. 1) are composed of straight segments, then the Ω-plane also is composed of straight lines. In other words, the flow retains a constant

direction along the solid boundaries (lines parallel to the logarithmic axis in the Ω-plane), and a constant velocity along the free surfaces (lines normal to the logarithmic axis in the Ω-plane). Since such a polygonal boundary can always be transformed onto a t-plane through the use of the Schwarz-Christoffel transformation, all two-dimensional jet-deflection problems of this nature may be, at least theoretically, solved.

It is also apparent from the foregoing that whenever both the magnitude and the direction of the velocity vary along a rigid boundary, then the Ω-plane is not in general composed of straight lines or of lines conveniently intersecting each other at 90 or 180 degree angle. In general if the curved boundaries in the physical plane is given, then the corresponding portion of the Ω-plane will be an unknown curve since the magnitude of the velocity is not initially known. One may, therefore, attempt to simplify the problem, for example, by specifying the variation of the magnitude of the velocity along the boundary. This does not in any way alleviate the difficulties to be encountered later since there does not exist a transformation function comparable to that given by Schwarz and Christoffel which could transform an Ω-plane composed in part by curved segments onto a t-plane in which the potential-function may be written. Consequently, one will either seek other methods of handling the curved boundaries or completely abandon the direct approach of obtaining a solution for a given geometry. The indirect

approach called into action will seek a family of solutions for a family of initially unknown curved boundaries and then will let the designer choose one among those obtained to suit his desired needs. In the following, the efforts made by others in rounding the corners of buckets otherwise composed of straight lines and the efforts to obtain indirect solutions will be described.

B. ROUNDING OF THE CORNERS AND BOUNDARIES

Because of its theoretical as well as technological importance, the problem of rounding the sharp corners on rigid boundaries over or through which the fluid flows has attracted the attention of many mathematicians and hydrodynamicists. Prior to a brief exposition of these efforts, it should be noted that there has not been, up to now, a sufficiently general method of studying the flow around curved bodies and that the techniques so far developed are not only difficult to handle but also require the use of special techniques for a given problem.

1. Curved Walls of Constant Pressure

As cited earlier, both the magnitude and the direction of velocity vary along a curved boundary and the functional relationship between the wall geometry and the vector velocity is not known a priori. However, by making a simplifying assumption such that the pressure or the total velocity along the curved wall remains constant, one can round the corners in a bucket otherwise composed of straight segments.

The method may best be described by applying it to the U-shaped bucket case discussed earlier.

Let the Ω-plane (see Fig. 1c) be modified in such a manner so that it takes the shape shown in Fig. 2a. Evidently the magnitude of velocity along $\overline{PQ}$ remains constant and the direction varies from $\pi/2$ at P to π at Q. The Ω-plane is still composed of straight lines and may, therefore, be transformed into either the upper or the lower half of a t-plane through the use of the Schwarz-Christoffel transformation. The remainder of the analysis will not be presented here. Suffice it to say that the transformation now involves two additional terms in the form of $\sqrt{t-t_p}$ $\sqrt{t-t_q}$ and, therefore, renders the succeeding integrations relatively more difficult to perform. Be that as it may, the method is in principle capable of generating curved corners along which the pressure or the velocity remains constant. There is sufficient flexibility in the analysis to move the points A and Q along the boundaries to obtain smaller or larger curved corners within reasonable limits.

2. Curved Walls with Special Pressure Distributions

A bolder approach to the modification of the Ω-plane is its modification in such a manner that while the direction of flow along the curved wall varies linearly, the magnitude of the velocity varies logarithmically. This procedure still allows the Ω-plane to be composed of straight segments (see Fig. 2b). It is immediately apparent that the application

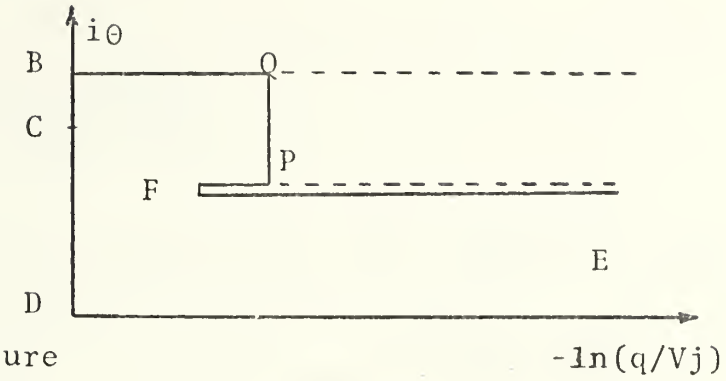

(a) Ω-plane for constant pressure curvature

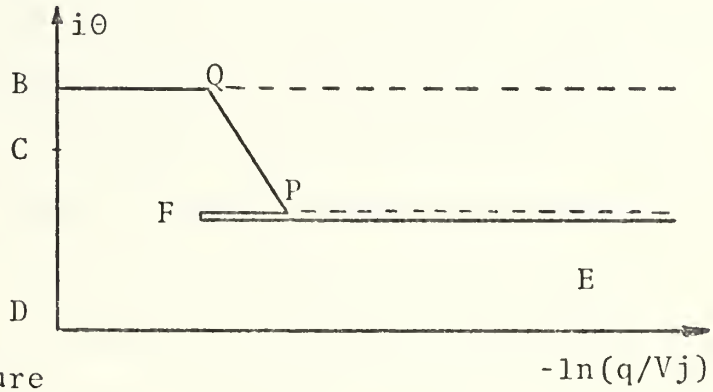

(b) Ω-plane for variable pressure curvature

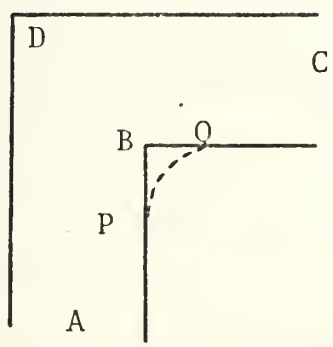

(c) Ω- or z-plane

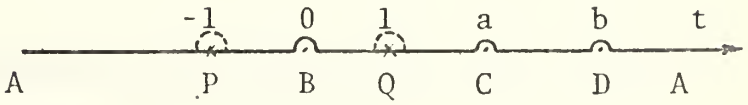

(d) t-plane with modifications at P and Q

Figure 2 Modifications of the Ω- and t-planes to round the corner

of the Schwarz-Christoffel transformation now yields terms such as

$$(t-t_p)^{\alpha_p/\pi} \quad (t-t_q)^{\alpha_q/\pi}$$

as a consequence of the fact that the line segments in the Ω-plane, no longer intersect each other normally. Only under rare circumstances, i.e. for special values of α_p or α_q, that the integral equation resulting from the Schwarz-Christoffel transformation may be integrated in terms of the Beta-functions. In general, the transformation may be integrated only numerically. Since the determination of the coordinates of the rigid boundaries in the physical plane requires another integration, similar to Eq. (8), the solution of the problem via a two-stage numerical integration becomes not only difficult but also quite approximate.

This method has been applied by Schieldrop [5] to the analysis of Borda-mouth-piece type flows with curved edges. The method is not in general easy to apply and requires a great deal of ingenuity and sophistication in numerical integrations.

3. Curved Walls Through the Modification of the t-plane

Cockcroft [6] introduced a method by means of which the corners of a solid boundary may be slightly rounded by modifying the t-plane. Consider the flow in a 90 degree corner as shown in Fig. 2c. This plane may be regarded as either z or the Ω-plane. In the absence of round corners,

the Schwarz-Christoffel transformation relates this plane to the t-plane (see Fig. 2d) by

$$z \text{ or } \Omega = M_o \int \frac{\sqrt{t-0}\ dt}{(t-a)\ \sqrt{t-b}} + N_o \qquad (9)$$

The corner at B may be rounded in an indirect way by replacing $\sqrt{t-0}$ in the above equation by $\sqrt{t+1} + \lambda\sqrt{t-1}$. In this substitution the argument of $\sqrt{t}$ which changed to $\pi/2$ at $t = 0$ now varies smoothly when t moves from $t = -1$ to $t = +1$. In other words, a curve is produced in the z or Ω-plane whose curvature depends on the arbitrary value of λ. It should be noted that for a value of λ, say

$$\lambda = \sqrt{\frac{b+1}{b-1}}$$

the velocity or the pressure along the curved wall remains constant. In fact, evaluating dW/dz in the range of $-1 \leq t \leq 1$, one obtains

$$\left|\frac{dW}{dz}\right| = \frac{1}{a}\sqrt{\frac{b-1}{2}}$$

This method was successfully used by Cockcroft [6] in calculating the electrical-stress distribution around certain two-dimensional conductors. A brief discussion of this method and the difficulties associated with its applications are also described by Carrier et al. [7].

4. Curving of the Boundaries Through the Use of Special Transformations

The Riemann-Hilbert transformation has been extensively used by Larock and Street [8] in the analysis of flow about supercavitating hydrofoils and by Larock [9] in analyzing in an indirect manner the efflux from curved nozzles. The mathematical details of this method will be discussed further later in connection with its application to the jet deflection problem.

5. Analysis of Flow about Curved Bodies by Levi-Civita's Method

Because of its challenging nature, the question of the existence and uniqueness of potential flows past general obstacles, having boundaries of given shape, has intrigued many outstanding mathematicians such as Brillouin [10], Villat [11], Levi-Civita [12], and others. In fact, Levi-Civita may be said to have solved the inverse problem of describing the class of all jets divided by curved barriers. Although no specific solutions have been presented, the problem of determining such flows was reduced in special cases to the solution of nonlinear integral equations with appropriate boundary conditions. The solutions are obtained in general by solving such equations numerically and by suitably choosing the necessary number of parameters. Such parameters described for example the variation of the inclination of the velocity vector, the variation of the magnitude of velocity, etc. It is important to know that the present problem of the deflection of a two-dimensional jet from a curved

boundary has not been previously solved by any of the methods so far described.

In Section II, Levi-Civita's method, among others, will be described in greater detail in generating a family of curved buckets for a given jet and prescribed jet deflection angle.

C. SUMMARY

Major emphasis in the foregoing introduction has been on the direct or indirect analysis of the impingement of ideal fluids on two-dimensional straight or curved boundaries. These analyses are often difficult to apply and the amount of work required may not be commensurate with the need for a solution. In such cases, the use of relatively less-exact methods may be adequate or even necessary. For two-dimensional flows in general and for axisymmetric flows in particular approximate methods have been developed. A detailed discussion of these methods with the exception of the finite element method may be found in Robertson [13]. These methods may be classified as graphical (field plot or flow net), finite-difference numerical analysis (iteration, relaxation, Monte Carlo), and analogies (electrical analogy, Hele Shaw, and membrane analogy), and finally the finite element method. The first three of these approximate methods have been widely used and amply described by Robertson [13]. The finite element method which came into existence during the past decade is currently being applied to the solution of

two-dimensional and axisymmetric Laplace-field problems. A detailed discussion of this method and its application to axisymmetric jet deflection problems will be presented in Section III. In the following, exact methods of analysis of the deflection of two-dimensional jets from curved buckets will be undertaken.

II. ANALYSIS OF TWO-DIMENSIONAL JET DEFLECTION FROM CURVED BUCKETS

In the following, three methods will be employed to obtain a family of curved-bucket shapes in terms of a given jet deflection angle and the angle of departure at the lip of the two-dimensional bucket. The jet will be assumed to be free and impinging symmetrically upon the bucket. These methods consist of the modified hodograph-method, Levi-Civita's method, and the Riemann-Hilbert method. The first of these is novel and the other two have been previously employed as discussed in Section I.B.

A. MODIFIED HODOGRAPH METHOD

The method consists of the definition of the hodograph-plane, its transformation into an infinite strip, and subsequently, into a t-plane through the use of the Schwarz-Christoffel transformation. The flow in the t-plane is expressed in terms of appropriate singularities and then the geometry of the curved bucket is determined through the evaluation of the proper integrals.

Consider the hodograph-plane in Fig. 3b where

$$\zeta = -\frac{1}{V_j}\frac{dW}{dz} = \frac{q}{V_j}e^{-i\theta} \qquad (10)$$

The fluid stagnates at A, accelerates along $\overline{ANB}$ in a manner specified by the hodograph-plane, leaves the bucket at B at

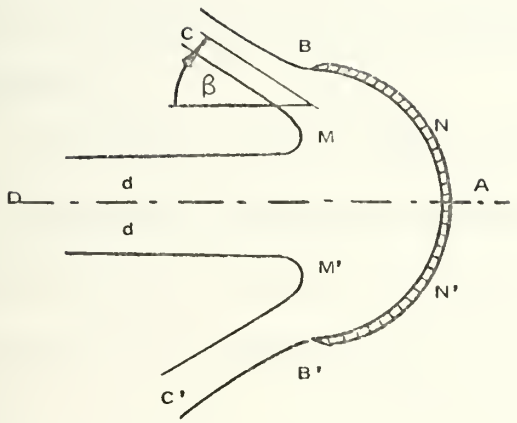

(a) z-plane

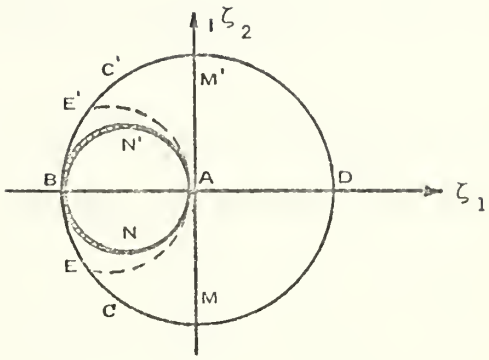

(b) ζ-plane

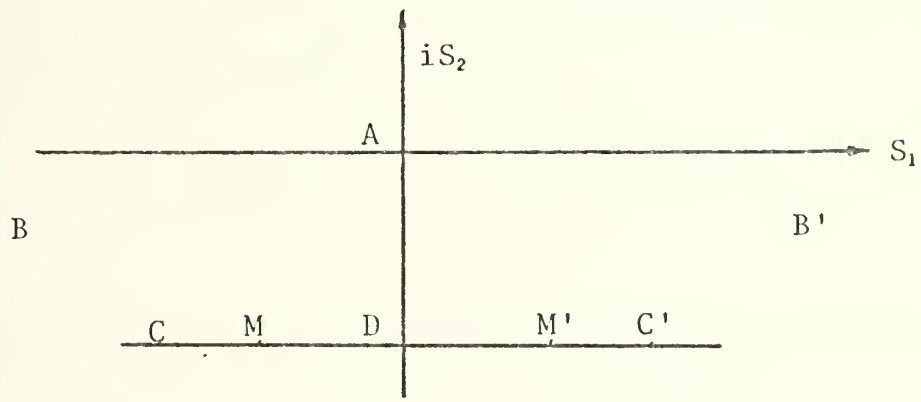

(c) S-plane

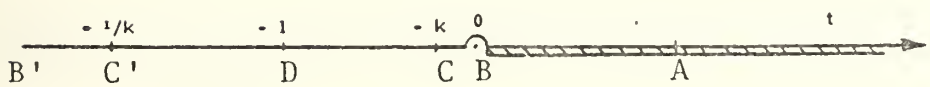

(d) t-plane

Figure 3 Transformation planes for the modified-hodograph method

an angle of π, and eventually acquires an angle of deflection β. Thus, the outer unit circle in the hodograph-plane represents the free streamlines of constant velocity. As stated earlier, the fluid is assumed to be inviscid and the real-fluid effects such as boundary layer, entrainment, etc. are ignored.

Clearly, the arc $\overline{ANB}$ in the hodograph plane may be chosen to represent different velocity variations along the bucket and different angles of departure at B, e.g., the curve $\overline{AE}$. Although the analysis will be relatively more complex, there are, to be sure, no conceptual difficulties and differences between that presented herein and other cases.

The hodograph-plane may be transformed to an S-plane (see Fig. 3c) through

$$S = - \frac{2 i \zeta}{\zeta + 1} \tag{11}$$

and the interior of the polygon in the S-plane may be transformed into the lower half of the t-plane by

$$S = \frac{1}{\pi} \ln t \tag{12}$$

which is obtained through the use of the Schwarz-Christoffel transformation.

The flow in the t-plane is comprised of two sinks and a source. Hence the complex potential is given by

$$W = \frac{V_j d}{\pi}[\ln(t+k) + \ln(t+\frac{1}{k}) - 2\ln(t+1)] \qquad (13)$$

Writing

$$dz = -\frac{1}{V_j}\frac{1}{\zeta}\,dW$$

to obtain the geometry of the bucket, one has

$$dz = \frac{d}{\pi}[1 + \frac{2i\pi}{\ln t}] \cdot [\frac{1}{t+k} + \frac{1}{t+\frac{1}{k}} - \frac{2}{t+1}]\,dt \qquad (14)$$

After separation of the real and imaginary part, one obtains

$$\frac{x}{d} = \frac{1}{\pi}\ln\frac{(t+k)\,(t+\frac{1}{k})}{(t+1)^2}\Bigg|_1^x \qquad (15)$$

and

$$\frac{y}{d} = -2\int_1^t \frac{1}{\ln t}\,(\frac{1}{t+k} + \frac{1}{t+\frac{1}{k}} - \frac{2}{t+1})\,dt \qquad (16)$$

The deflection angle β is related to the parameter k through

$$k = \mathrm{EXP}\,(-\pi\frac{\sin\beta}{1-\cos\beta}) \qquad (17)$$

which is obtained by writing $\zeta = e^{-i\beta}$, inserting it in Eq. (11) and combining with Eq. (12).

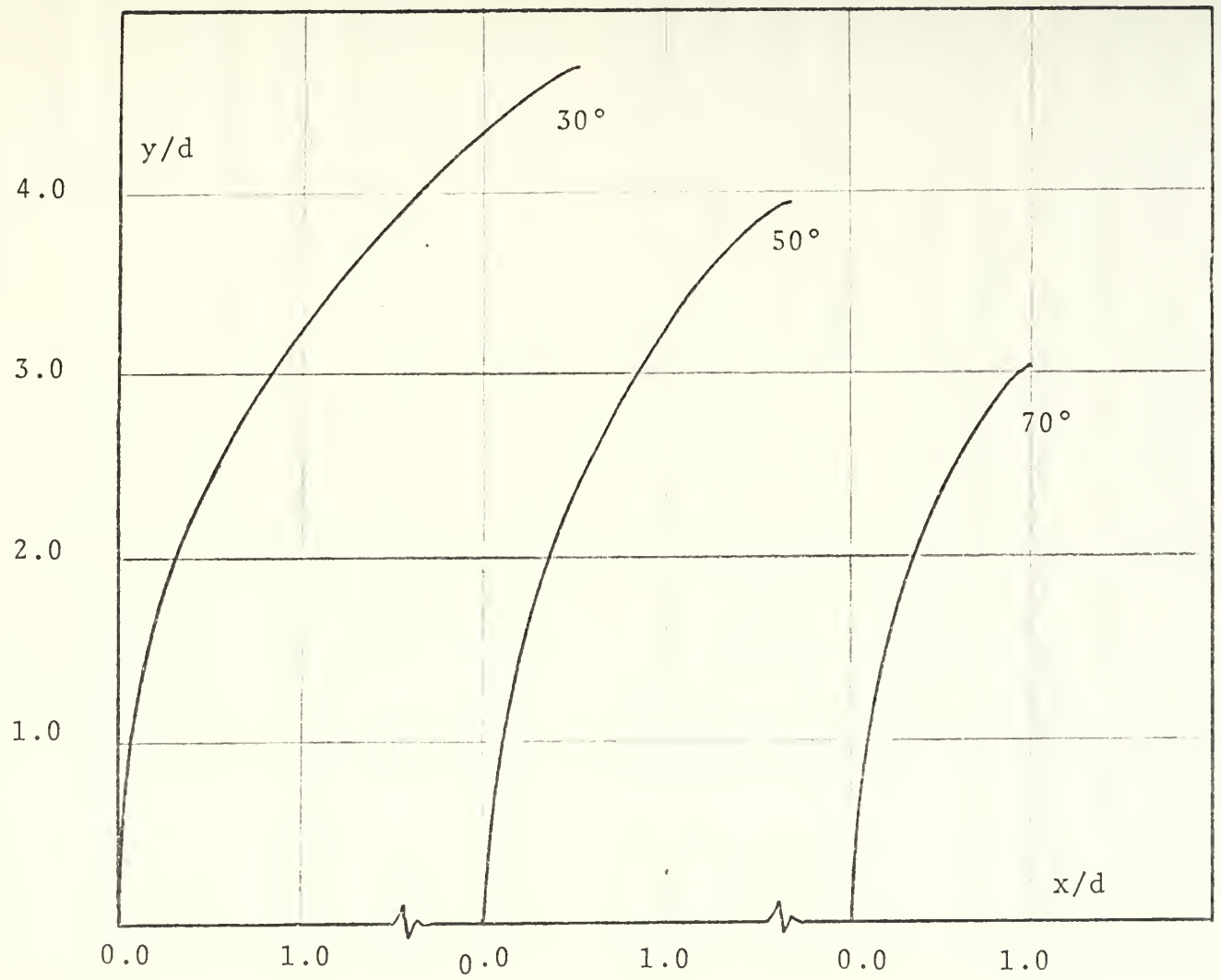

Figure 4 Family of buckets obtained via modified-hodograph method

The foregoing completes the formal analysis of the problem. The bucket geometry may now be calculated for a given deflection angle β through the use of Eqs. (15), (16) and (17). The results obtained through a straightforward integration scheme are shown in Fig. 4 for a set of representative jet deflection angles. The coordinates of the 50 degree case are shown in Appendix A, and the computer program in Appendix B. Suffice it to say that the thrust acting on the bucket may easily be determined through the use of the momentum equation in terms of the deflection angle β.

B. LEVI-CIVITA'S METHOD

This method, which is fully described in several reference texts (e.g. Birkhoff and Zarantonello [14], Milne-Thomson [4]), consists of the definition of a complex function ω as

$$\omega = \theta + i \ln \left(\frac{q}{V_j}\right)$$

where θ and q are respectively the direction and the magnitude of the velocity vector. V_j is the constant velocity along the free streamlines. The ω-function is expressed in terms of a polynomial in such a manner that ω is real over the free streamlines and complex over the curved obstacle. The shape or the curvature of the obstacle is defined in terms of the coefficients of a polynomial representing ω.

Even though this method was originally devised to deal with curved boundaries, as discussed in Section I.B-5, its

application has been mostly restricted to boundaries with straight-line segments (Cisotti [15]), because of the analytical difficulties encountered in its application to curved boundaries. Wu [16] has employed it in the study of flow about fully-cavitating, slightly-curved, hydrofoils.

The physical z-plane (see Fig. 5a) consists of a jet of width 2d and velocity V_j impinging upon a curved, symmetric, two-dimensional bucket $\overline{BAB'}$. The complex-potential function W is given as usual by (see Fig. 5b)

$$W = \phi + i\psi \tag{15}$$

A straightforward application of the Schwarz-Christoffel transformation establishes a relation between the t- and W-planes. Thus, one has

$$W = -\frac{V_j d}{\pi} [\ln (1-t) + \ln (1+t)] \tag{19}$$

Because of the symmetry, t is taken equal to +1 and -1 at C and C' respectively and zero at A. The parameter k is assigned to B and, as will be shown later, it is uniquely related to the deflection angle β.

The upper half of the t-plane is transformed into the inner region of a semicircle of unit radius (Fig. 5c) through the transformation given by Levi-Civita [12] as

$$t = -\frac{k}{2} \left(\zeta + \frac{1}{\zeta}\right) \tag{20}$$

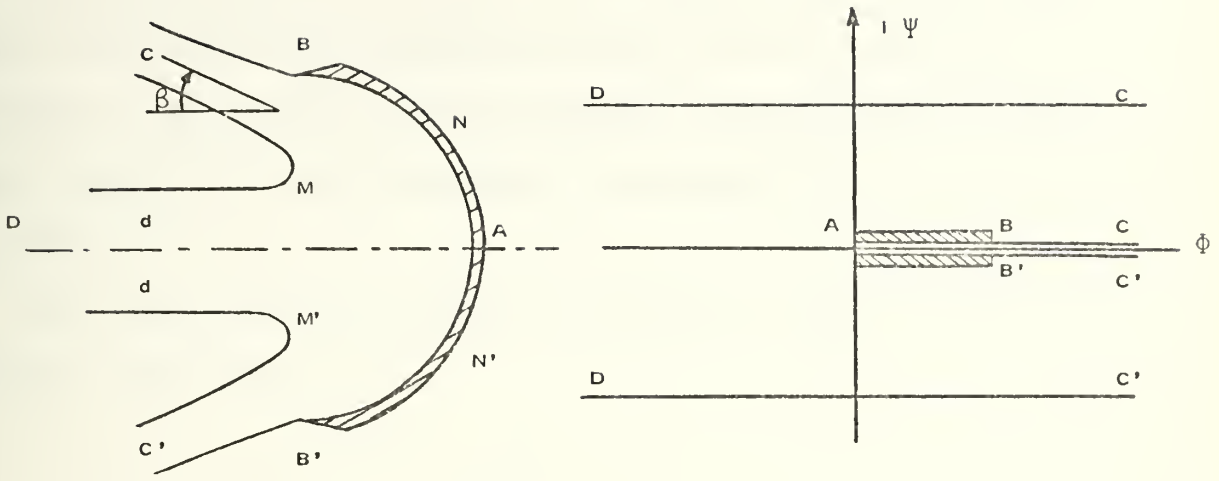

(a) z-plane (b) W-plane

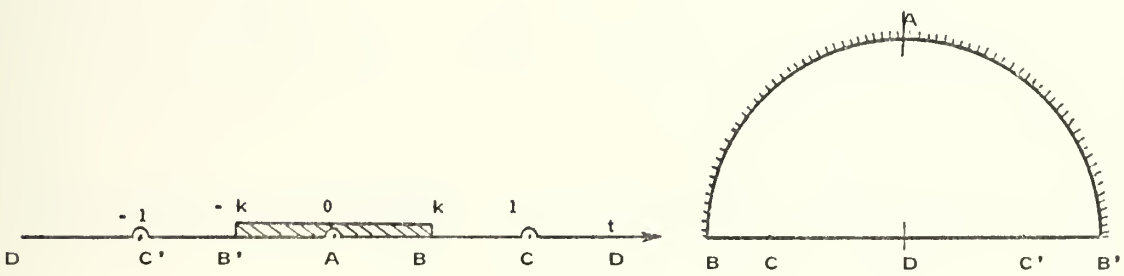

(c) t-plane (d) ζ-plane

Figure 5 Transformation planes for Levi-Civita's method

The circular arc $\overline{BAB'}$ in Fig. 5c represents the solid boundary over which the direction of the velocity vector is assumed to be prescribed and diametric line $\overline{BCDC'B'}$ represents the free streamlines where the magnitude of the velocity is known.

The relationship between the points in the z, t and ζ-planes are given by:

$$\begin{aligned} &\text{point } B', \quad t = -k, \quad \zeta = +1 \\ &\text{point } A\ , \quad t = 0, \quad \zeta = i \\ &\text{point } D\ , \quad t \to \infty, \quad \zeta = 0 \\ &\text{point } B\ , \quad t = k, \quad \zeta = -1 \end{aligned} \tag{21}$$

The W-plane is related to the z-plane, as before, by

$$-\frac{1}{V_j}\ \frac{dW}{dz} = \frac{q}{V_j}\, e^{-i\theta} \tag{22}$$

where q and θ represent respectively the magnitude and direction of the velocity vector.

One can now define an ω-function which is quite similar to that given by Planck as

$$\omega = i \ln \left(-\frac{1}{V_j}\ \frac{dW}{dz}\right) = \theta + i \ln \left(\frac{q}{V_j}\right) \tag{23}$$

Now solving for z in the above equation and expressing all the variables as functions of ζ one has

$$\frac{z}{d} = -\frac{1}{V_j} \int e^{i\omega(\zeta)} \frac{dW}{d\zeta} d\zeta \qquad (24)$$

Defining

$$\zeta = r\, e^{i\sigma}$$

and noting that over the bucket only the argument and along the free streamlines only the modulus varies, the combination of Eqs. (19) and (24) yields,

$$\frac{z}{d} = \frac{1}{\pi} \cdot \int e^{i\omega(\sigma)} \left[\frac{2k^2 \cos\sigma \sin\sigma}{1 - k^2 \cos^2\sigma}\right] d\sigma \qquad (25)$$

and

$$\frac{z}{d} = \frac{1}{\pi} \cdot \int e^{i\omega(r)} \left[\frac{\frac{k^2}{2r}\left(r^2 - \frac{1}{r^2}\right)}{\frac{k^2}{4}\left(r + \frac{1}{r}\right)^2 - 1}\right] dr \qquad (26)$$

Equation (25) gives the coordinates of the bucket and Eq. (26) the coordinates of the free streamlines.

The function ω is assumed, according to Levi-Civita, to be of the form

$$\omega(\zeta) = i \ln \frac{i - \zeta}{i + \zeta} + a_o + a_1\zeta + a_2\zeta^2 + a_3\zeta^3 \ldots. \qquad (27)$$

where the logarithmic term can be identified as that corresponding to a free jet impinging normally upon a flat plate

(Cisotti[17]). The additional terms in the polynomial whose coefficients are to be prescribed later modifies the expression for ω and helps to curve the solid boundary.

Because of the symmetry of the flow in the physical plane, the coefficients a_o, a_2, a_4, ... are not acceptable.

Noting that over the solid boundary $r = 1$ and over the free streamlines $\sigma = 0$ or $\sigma = \pi$, Eq. (27) may be reduced over the bucket to

$$\omega(\sigma) = i \ln \frac{|\cos \sigma|}{1 + \sin\sigma} \pm \frac{\pi}{2} + a_1 e^{i\sigma} + a_3 e^{i3\sigma} + a_5 e^{i5\sigma} .... \tag{28}$$

where plus sign is to be used for $\pi > \sigma > \pi/2$, and minus sign for $\pi/2 > \sigma > 0$. Over the free streamlines, it reduces to

$$\omega(r) = - \tan^{-1} \frac{2r}{1 - r^2} + a_1 r + a_3 r^3 + a_5 r^5 \ ... \tag{29}$$

The coefficients a_1, a_3, a_5, ... may now be chosen to obtain different bucket shapes. In the present study, ω is chosen to satisfy the following conditions

$$\begin{aligned} \omega(+1) &= -\pi \\ \omega(i) &= \pm \frac{\pi}{2} - i \infty \\ \omega(-1) &= \pi \\ \omega(o) &= 0 \end{aligned} \tag{30}$$

These conditions simply state that the jet departure angle at the lip of the bucket be equal to $\pm\pi$, and that the bucket be continuous in curvature at the stagnation point A and symmetric with respect to the jet axis.

There are several ways to select the coefficients a_i. In this study a Fourier-series representation was used primarily because of the versatility afforded by it in representing different bucket shapes.

Equation (28) can be written over the circular arc $\overline{AB'}$ as

$$\omega(\sigma) = i\{\ln \frac{\cos \sigma}{1 + \sin\sigma} + a_1 \sin\sigma + a_3 \sin 3\sigma + a_5 \sin 5\sigma \ldots\}$$
$$+\{-\frac{\pi}{2} + a_1 \cos \sigma + a_3 \cos 3\sigma + a_5 \cos 5\sigma \ldots\} \qquad (31)$$

The real part of Eq. (31) represents the direction θ of the velocity vector over the bucket. Thus, it is obvious that, one can prescribe the curvature of the bucket or the modulus of the velocity vector by properly choosing the coefficients a_1 through a_n.

Let θ be represented by the lines shown in Fig. 6. Evidently, by choosing sufficient number of terms, one can represent the variation of θ with σ shown in Fig. 6. In doing so it is important to make θ symmetric with respect to the θ axis since the series are expressed in cosine terms only.

Rewriting Eq. (31) one has over the arc $\overline{AB'}$

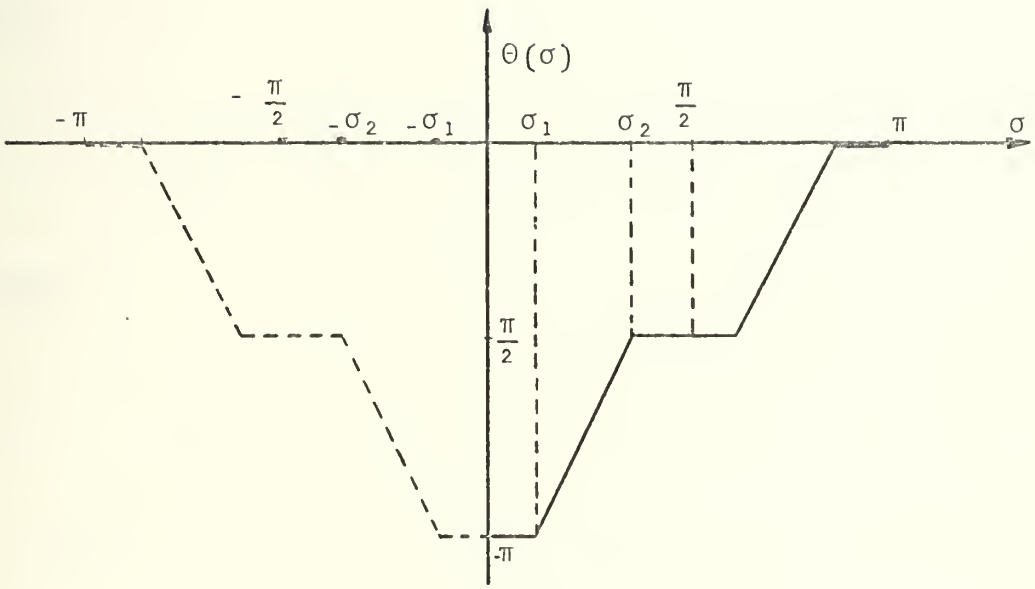

Figure 6 Approximate representation of $\Theta(\sigma)$

$$\omega(\sigma) = i \ln \frac{\cos \sigma}{1 + \sin \sigma} + i\, h(\sigma) + \theta(\sigma) \qquad (32)$$

where

$$h(\sigma) = \sum_{n=1}^{N} a_n \sin n\sigma \qquad (33)$$

and

$$\theta(\sigma) = -\frac{\pi}{2} + \sum_{n=1}^{N} a_n \cos n\sigma \qquad (34)$$

where

$$a_n = \frac{2}{(\sigma_1 - \sigma_2)n^2} [\cos n\sigma_1 - \cos n\sigma_2] \qquad (35)$$

in which σ_1 and σ_2 represent the two parameters shown in Fig. 6. The evaluation of the Fourier coefficients a_n is shown in Appendix C. To complete the analysis one needs to evaluate the term $e^{i\omega(\sigma)}$ which appears in Eq. (25) in terms of Eq. (32). Writing

$$e^{i\omega(\sigma)} = \frac{1 + \sin \sigma}{\cos \sigma} e^{-h(\sigma)} e^{i\theta(\sigma)}$$

and separating the real and imaginary parts, one has

$$e^{i\omega(\sigma)} = \frac{1 + \sin \sigma}{\cos \sigma} e^{-h(\sigma)} (\cos \theta(\sigma) + i \sin \theta(\sigma)) \qquad (36)$$

Now combining Eqs. (25), (33), (35) and (36), one finally obtains

$$\frac{x}{d} = \frac{1}{\pi} \int_{\pi/2}^{\sigma} e^{-h(\sigma)} \sin \theta(\sigma) \frac{2k^2 \sin \sigma(1 + \sin \sigma)}{1 - k^2 \cos^2 \sigma} d\sigma \tag{37}$$

and

$$\frac{y}{d} = \frac{1}{\pi} \int_{\pi/2}^{\sigma} e^{-h(\sigma)} \cos \theta(\sigma) \frac{2k^2 \sin \sigma(1 + \sin \sigma)}{1 - k^2 \cos^2 \sigma} d\sigma \tag{38}$$

Equations (37) and (38) yield the coordinates of each segment of the curved boundary through the use of the appropriate values of σ_1 and σ_2. This in essence completes the application of the Levi-Civita's method to the analysis of the jet deflection from curved obstacles. In the following the implications of the variations of σ_1 and σ_2 will be discussed.

The variation of θ with σ shown in Fig. 6 may be written for each interval as

$$\begin{aligned}
&\theta(\sigma) = -\pi \qquad 0 < \sigma < \sigma_1 \\
&\theta(\sigma) = \frac{\pi}{2} \left(\frac{\sigma}{\sigma_2 - \sigma_1}\right) - \frac{\pi}{2} \left(2 + \frac{\sigma_1}{\sigma_2 - \sigma_1}\right) \qquad \sigma_1 < \sigma < \sigma_2 \\
&\theta(\sigma) = -\frac{\pi}{2} \qquad \sigma_2 < \sigma < \frac{\pi}{2} \\
&\theta(\sigma) = -\frac{\pi}{2} \qquad \frac{\pi}{2} < \sigma < \pi - \sigma_2
\end{aligned} \tag{39}$$

$$\theta(\sigma) = \frac{\pi}{2}\left(\frac{\sigma}{\sigma_2 - \sigma_1} - \frac{\pi - \sigma_1}{\sigma_2 - \sigma_1}\right) \qquad \pi - \sigma_2 < \sigma < \pi - \sigma_1$$

$$\theta(\sigma) = 0 \qquad \pi - \sigma_1 < \sigma < \pi$$

It will be shown that this particular functional dependence produces bucket geometries of the form shown in Fig. 7.

Rewriting Eqs. (37) and (38) for the particular example under consideration one has

$$\frac{x_p}{d} = 0 \tag{40a}$$

and

$$\frac{y_p}{d} = \frac{2}{\pi}\int_{\pi/2}^{\sigma_2} e^{-h(\sigma)}\,\frac{k^2 \sin\sigma(1 + \sin\sigma)}{1 - k^2\cos^2\sigma}\,d\sigma \tag{40b}$$

for the interval of $\frac{\pi}{2} > \sigma > \sigma_2$, i.e. for the segment $\overline{AP}$, (see Fig. 7)

$$\frac{x}{d} = \frac{2}{\pi}\int_{\sigma_2}^{\sigma} e^{-h(\sigma)}\,\frac{k^2 \sin\sigma(1 + \sin\sigma)}{1 - k^2\cos^2\sigma}\cos\left[\frac{\pi}{2}\,\frac{\sigma - \sigma_1}{\sigma_2 - \sigma_1}\right]d\sigma \tag{41a}$$

and

$$\frac{y}{d} = \frac{2}{\pi}\int_{\sigma_2}^{\sigma} e^{-h(\sigma)}\,\frac{k^2 \sin\sigma(1 + \sin\sigma)}{1 - k^2\cos^2\sigma}\sin\left[\frac{\pi}{2}\,\frac{\sigma - \sigma_1}{\sigma_2 - \sigma_1}\right]dr + y_p \tag{41b}$$

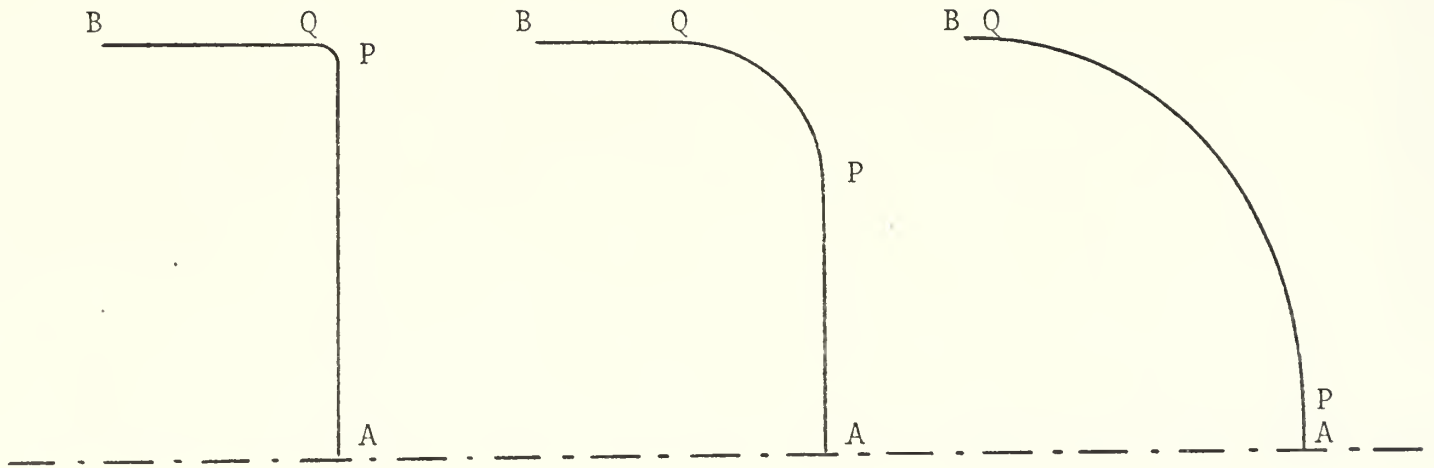

Figure 7 Schematic representation of three different bucket shapes

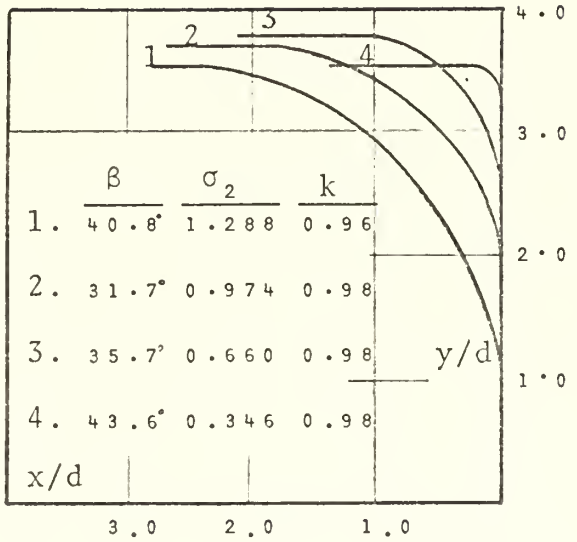

(a) Family of curved buckets for $\sigma_1 = 0.31416$

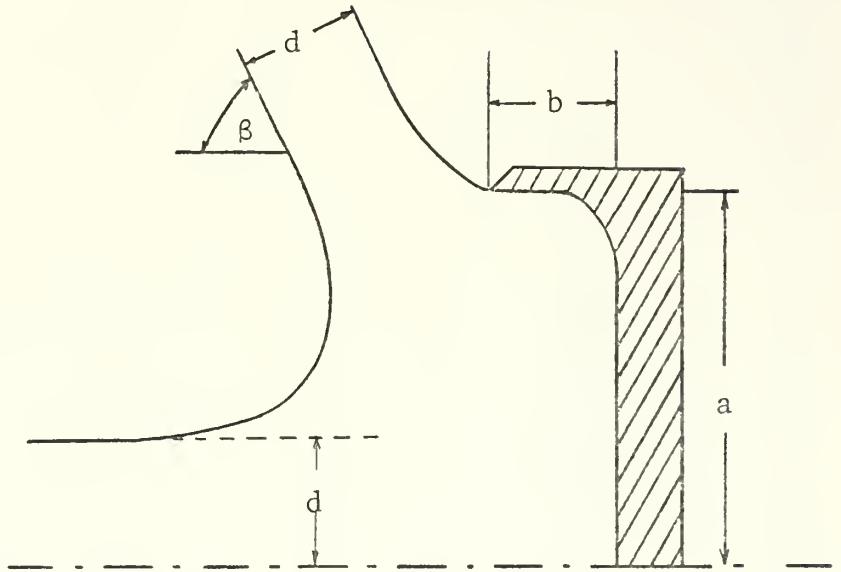

(b) A curved bucket and free streamlines
$\sigma_1 = 0.31416$, $\sigma_2 = 0.47124$, k=0.946
a/d=3.05 , b/d=1.07 , $\beta = 68$ deg.

Figure 8 Family of curved buckets obtained by Levi-Civita's method

for the interval $\sigma_2 > \sigma > \sigma_1$, i.e. for the curved segment $\overline{PQ}$, and finally

$$\frac{x}{d} = \frac{2}{\pi} \int_{\sigma_1}^{0} e^{-h(\sigma)} \frac{k^2 \sin(1 + \sin\sigma)}{1 - k^2 \cos^2\sigma} d\sigma + x_q \qquad (42a)$$

and

$$\frac{y}{d} = y_q \qquad (42b)$$

for the interval $\sigma_1 > \sigma > 0$, i.e. for the segment $\overline{QB}$.

The coordinates of the free streamlines may be obtained by integrating Eq. (26) through the use of Eq. (29) and the coefficients a_i given by Eq. (37). Finally, the deflection angle is evaluated by replacing in Eq. (29) the corresponding value of r at the point C, i.e. $r = \frac{1}{k}(1 - \sqrt{1 - k^2})$.

The foregoing equations have been numerically integrated (the computer program is given in Appendix D), and the resulting family of bucket shapes are shown in Fig. 8a. A special case for $\sigma_1 = 0.31416$, $\sigma_2 = 0.47124$, and $k = 0.946$ is shown in Fig. 8b.

C. RIEMANN-HILBERT METHOD

The method consists of the transformation of the physical plane into the W-plane, where W is given by

$$W = \phi + i\,\psi$$

and the transformation of the W-plane into the upper half of a t-plane through the use of the Schwarz-Christoffel transformation. Then the flow in the t-plane, which is composed of segments of solid boundaries and free streamlines are related to the Riemann-Hilbert transformation as a well-posed mixed boundary value problem. Then a certain shape function f(t) is assumed and the characteristics of the flow in the physical plane are evaluated through integration.

The details of the technique will become clear as it is applied to the determination of the deflection angle of a two-dimensional jet impinging symmetrically upon a two-dimensional bucket.

Figure 9a shows a jet of width 2d impinging upon a curved bucket with a 180 degree angle of departure at the upper and lower lip of the bucket.

It is apparent from the application of Bernoulli's equation that the velocity is constant along the free surfaces. The complex-function W, for the upper half of the physical plane, is represented by an infinite slit as shown in Fig. 9b. The W-plane can in turn be transformed into the upper half of a t-plane through the use of the Schwarz-Christoffel transformation. The straightforward application of this transformation yields

$$W(t) = \frac{V_j d}{\pi} \ln t \qquad (42)$$

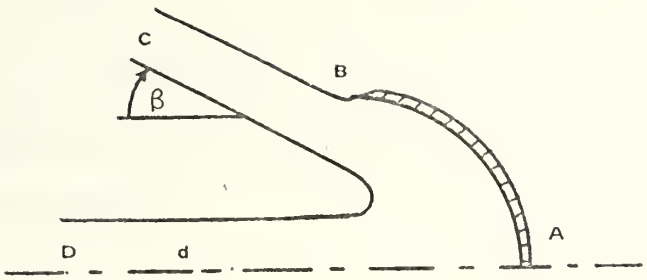

(a) z-plane

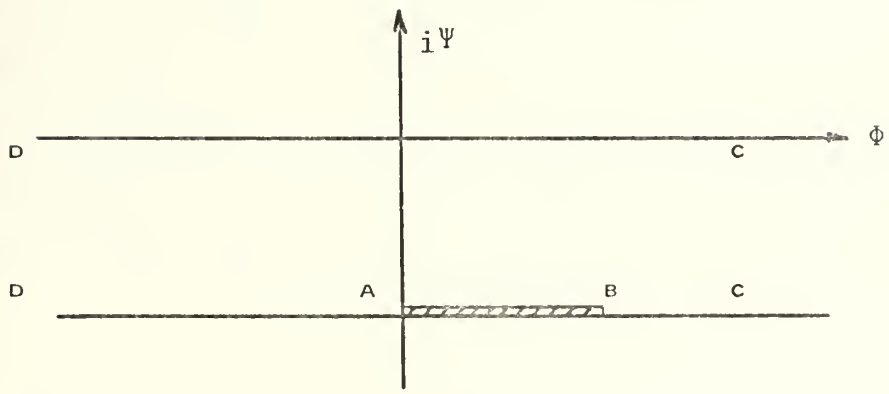

(b) W-plane

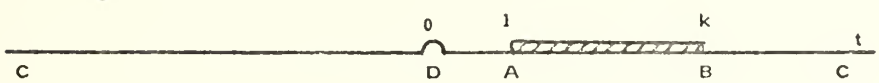

(c) t-plane

Figure 9 Transformation planes for the Riemann-Hilbert method

where V_j is the velocity along the free surfaces. In accordance with the rule of this transformation, three of the t values are assigned arbitrary values (t = 1 at A, t = $+\infty$ at C and t = 0 at D), and an unknown parameter k is assigned to the point B.

The complex-potential-function W is related to the physical z-plane by

$$\frac{dW}{dz} = -q\, e^{-i\theta} \tag{43}$$

where q and θ represent respectively the magnitude and the direction of the velocity vector.

It is convenient at this point to separate the magnitude and the direction of the velocity through the application of Planck's logarithmic transformation given by

$$\omega = \ln \frac{q}{V_j} - i\,\theta \tag{44}$$

Combining Eqs. (42) and (44) and solving for z in terms of t, one has

$$\frac{z}{d} = -\frac{1}{\pi} \int e^{-\omega(t)}\, \frac{dt}{t} \tag{45}$$

It is apparent from the foregoing development that the real part of the complex-function $\omega(t)$ is zero along the free streamlines where $q = V_j$. Thus,

$$\mathrm{Re}[\omega(t)] = 0 \quad \text{for} \quad t > k \quad \text{and} \quad t < 0$$

The imaginary part of $\omega(t)$ which represents the direction of the velocity vector is zero along the line $\overline{AD}$ where $0 < t < 1$. Over the bucket, however, both the magnitude and the direction of the velocity are variable and are an unknown function of t. Let this function be denoted by $f(t)$ in the interval $1 < t < k$.

The foregoing conditions define a well posed Riemann-Hilbert mixed-boundary value problem where the real and imaginary parts of an analytic function $\omega(t)$ are alternately known along the real axis, i.e.,

$$\begin{aligned} &\mathrm{Re}(\omega) = 0 \qquad t > k \\ &\mathrm{Im}(\omega) = -f(t) \qquad 1 < t < k \\ &\mathrm{Im}(\omega) = 0 \qquad 0 < t < 1 \\ &\mathrm{Re}(\omega) = 0 \qquad t < 0 \end{aligned} \tag{46}$$

The general solution of the Riemann-Hilbert problem is well known (Cheng and Rott [18] and Larock [9]).

In principle one writes

$$\omega(t) = H(t)\, Q(t) \tag{47}$$

where H(t) is the solution of the homogeneous-Riemann problem (i.e. for f(t) = 0) as it satisfies all the other conditions listed in Eq. (46) and may be chosen as

$$H(t) = \sqrt{-t(t - k)} \tag{48}$$

In passing it should be noted that the particular form of H(t) which constitutes a solution for f(t) = 0 is not of special importance as shown by Song [19] and that uniqueness of the solution does not depend on the particular value of H(t).

The function Q(t) may be written as (Larock [9])

$$Q(t) = \frac{1}{\pi} \int_{-\infty}^{+\infty} \frac{\mathrm{Im}[Q(\eta)]}{\eta - t} \, d\eta \tag{49}$$

Combining Eqs. (46), (47) and (48), one has

$$\omega(t) = \frac{\sqrt{-t(t - k)}}{\pi} \int_{1}^{k} \frac{-f(\eta)}{\sqrt{-\eta(\eta - k)}} \frac{d\eta}{(\eta - t)} \tag{50}$$

The remainder of the analysis depends on the selection of f(t). As pointed out earlier, f(t) would have been known had the shape of the solid boundary been known a priori. The present analysis, however, is an indirect approach and seeks the shape of the boundary in terms of the boundary conditions assigned and the deflection angle assumed. Thus, it is apparent that one may select f(t) as an arbitrary function

of t provided that the boundary conditions at the stagnation point and at the lip of the bucket are satisfied, and obtain a family of bucket shapes. In the following, f(t) will be taken as a linear function of t partly for the sake of simplicity and partly in order not to obscure the application of the method by introducing rather complex and unmanageable integrals. Thus, writing,

$$f(t) = a + bt \tag{51}$$

and choosing a and b in such a manner that the slope of the bucket be $\pm \pi/2$ at the point A and $\pm \pi$ at the lip, one has

$$a = \frac{\pi}{2} \frac{k - 2}{k - 1}$$

and

$$b = \frac{\pi}{2} \frac{1}{k - 1}$$

Inserting Eq. (51) in Eq. (50) one obtains

$$\omega(t) = \frac{\sqrt{-t(t - k)}}{\pi} \int_1^k \frac{-(a + b\eta)}{\sqrt{-\eta(\eta - k)}} \frac{d\eta}{\eta - t} \tag{52}$$

The integration of Eq. (52), the details of which are presented in Appendix E, yields,

$$\omega(t) = i\,\frac{(a + bt)}{\pi}\cos^{-1}\left[\frac{\frac{2}{k}t - t - 1}{t - 1}\right] - i\,\frac{b}{\pi}\sqrt{t(t-k)}\;\cos^{-1}\left[\frac{2-k}{k}\right] \tag{53}$$

for $t < 0$, and $t > k$

and

$$\omega(t) = -\frac{(a + bt)}{\pi}\ln\frac{\frac{k}{2}(t+1) - t + \sqrt{k-1}\,\sqrt{t(k-t)}}{\frac{k}{2}(1 - t)} - \frac{b}{\pi}\sqrt{t(k-t)}\;\cos^{-1}\left[\frac{2-k}{k}\right] \tag{54}$$

for $0 < t < k$

The deflection angle β can be found by letting $t \to -\infty$ in Eq. (53), or by letting $t \to \infty$ in Eq. (50) and then performing the integration as shown in Appendix F. The deflection angle β is found to be uniquely related to the parameter k as

$$\beta = \pi + \frac{1}{2(k-1)}\left[\left(\frac{3k}{2} - 2\right)\cos^{-1}\frac{2-k}{k} + \sqrt{k-1}\right] \tag{55}$$

To obtain the shape of the bucket and the actual location of the free streamlines, Eqs. (53) and (54) are replaced in Eq. (45) and integrated.

The integration must be performed numerically using the method described by Hartree [20] because of the singularity at the point $t = 1$. It must be pointed out that the singularity at $t = 1$ is an integrable singularity of the form

$$\int_0^1 \frac{dx}{\sqrt{x}}$$

No attempt is made here to perform the numerical integration of Eq. (45) even though the procedure is well known as shown in one application by Tinney [2], because the method previously described, namely, Levi-Civita's method, is very similar to the one presented herein and has the advantage of being very flexible to obtain different bucket shapes and presents no singularities for the integration.

D. A CRITIQUE OF THE ANALYTICAL METHODS FOR TWO-DIMENSIONAL FLOWS

The past as well as the present analyses have emphatically demonstrated that almost all of the difficulties of the analysis of jet deflection from curved obstacles are ascribable to the determination of the initially unknown free streamlines. In view of this fact a direct analysis of the problem, that is, the determination of the jet deflection and the position of the free streamlines via either purely analytical or partly analytical and partly numerical techniques is at best an exceedingly complex proposition. As propounded by Birckhoff et al. [14] and other hydrodynamicists what one can hope for is an indirect solution of the problem; that is, obtaining a family of obstacle shapes which will yield the prescribed jet deflection angle and provide a familiarity between the shapes so obtained and the range and change of direction of the free parameters involved in the analysis. What has been said so

far holds true for both the plane and axisymmetric flows. Should one adopt a purely numerical procedure (finite difference, relaxation, finite element, etc.) it is then and only then that it is possible to begin with a prescribed obstacle shape and to approach a unique solution through successive iterations.

In what follows, attention will be focused only upon the evaluation of the individual as well as relative merits of the analytical methods dealing with the deflection of plane jets.

The hodograph-method developed herein is capable, within the limitations of the potential-flow theory, of analyzing the flow in curved obstacles and generating a family of practically suitable bucket shapes. Furthermore, this method has the inherent capability of being extended to the generation of even a larger family of obstacle-shapes through the use of distributed sources and sinks in the hodograph-plane. Even though this concept has not been pursued further herein, there are no conceptual difficulties in doing so.

The method devised by Levi-Civita and successfully employed herein requires the judicious selection of the variation of θ with σ and the use of a suitable series to enable one to perform the integrals leading to the coordinates of the obstacle as well as of the free surfaces. The deflection angle may be determined either by calculating the asymptotic slope of the free streamlines or by finding the pressure distribution over the bucket and using the equation of

momentum. The emerging fact is that a brief familiarity with this method enables one not only to generate a family of suitable curved obstacles but also to round the corners of buckets composed of straight segments. For example, by letting $(\sigma_1 - \sigma_2) \to 0$ one finds that the bucket shape generated by this method exactly approaches that previously solved by Sarpkaya [1] (see Figure. 8a). For slightly larger values of $(\sigma_1 - \sigma_2)$ the corner $\overline{PQ}$ (see Fig. 7) is rounded, thus enabling one to evaluate the effect of the deviation of the segment $\overline{PQ}$ from a sharp corner on the deflection angle. In fact, the results show that for a given b/a and a/d ratios (see Fig. 1) the effect of the curvature is relatively small as anticipated by Sarpkaya [1] on the grounds that the flow of a real fluid near the sharp corners form nearly stagnant regions comprised of small corner vortices and provides a slightly rounded streamline.

Finally, it should be noted that Levi-Civita's method has been rendered practicable through the introduction of the Fourier-series into the analysis. It may be easily extended to the analysis of the cases where the lip angle of the bucket is other than π or the bucket has a cusp on its axis of symmetry or to the cases where the impinging jet is not free and emerges from a prescribed nozzle. Such shapes are known to be used in the design of spillways, Pelton wheels, two-dimensional cascading thrust-reversers, etc.

As to the Riemann-Hilbert method, it may have already been evident that it is in essence a mathematically more

elegant and sophisticated version of Levi-Civita's method in prescribing certain functions. It is for this reason that no particular solutions have been presented and only a linear variation of f(t) was studied. Needless to say, a quadratic or cubic variation of f(t) could have been employed. Evidently the resulting integrals would not have been integrable in closed form. Finally, it should be pointed out that the Riemann-Hilbert method is perhaps the only method aside from purely numerical methods with which one can incorporate into the analysis the effect of body forces such as gravity.

In closing the discussion of the methods dealing with the deflection of plane jets from curved obstacles, one must once more emphasize that all of the foregoing analyses and solutions deal with plane Laplace-field problems where the real-fluid effects must be out of necessity ignored. Because of the limitations imposed upon man's understanding of turbulence, the development of laminar and/or turbulent boundary layers under a nonzero pressure gradient along curved walls, entrainment between the jet and the surrounding fluid which may or may not have the same physical properties, and finally the Coanda effect (the tendency of jets to attach to adjacent surfaces because of the entrainment deprivation), the real-fluid effects on jet deflection cannot as yet be analyzed. It is because of these reasons that the analysis of the problem with the assumption of an inviscid fluid becomes more important for it is only through the comparison of such

solutions with the experimantal results that one can assess the degree of significance of the real fluid effects on the governing parameters. As stated in the introduction and as verified by numerous experiments (Robertson [13], p. 626), the phenomenon of jet deflection is governed primarily by pressure and inertia forces and that the real-fluid effects are of minor significance in determining the forces acting on the body and the deflection of the jet. These facts will be stressed again in connection with the discussion of the analytical and experimental results for axisymmetric jet deflection to be subsequently presented.

III. ANALYSIS OF AXISYMMETRIC JET IMPINGEMENT

A. INTRODUCTION

As stated in the general introduction, the two-dimensional counterpart of the jet-deflection problem has been treated by several investigators through the use of numerical and approximate analytical methods. Additional techniques based on the modified-hodograph method, Riemann-Hilbert integral transforms, and the Levi-Civita's method have been successfully developed and employed in the preceding section in the analysis of the jet impingement upon two-dimensional curved buckets.

The three-dimensional counterpart of the jet-deflection problem has not yet been solved in any generality. Attempts to formulate an exact solution have been mostly unsuccessful even for the axisymmetric inviscid flows with no body forces.

The case of a circular jet striking a plate normally was analyzed by Schaach [21] using approximate methods similar to those of Trefftz [22] with successive adjustment of the free streamlines and through the use of the Fredholm integral equations. These results are in good agreement with those obtained experimentally and to the surprise of the many investigators, they are almost identical to those of the two-dimensional cases.

Other noteworthy contributions to the analysis of the jet-efflux from nozzles and orifices with straight boundaries were made by Southwell and Vaisey [23], Rouse and Abul-Fetouh

[24], Garabedian [25], and Hunt [26] through the use of the relaxation and finite difference techniques, and singular-integral equations. Schnurr et al. [27] used the relaxation method to analyze the turning of two-dimensional and axisymmetric jets from curved surfaces where there was only one free stream surface; i.e. the jet was assumed to leave the deflector exactly parallel to the tangent at the lip of the deflector surface with a uniform velocity distribution and the consequences of the difference between the actual deflection angle and the said tangent to the deflector surface was taken as a measure of the "spillage" and expressed in terms of a "turning-effectiveness coefficient" determined experimentally. Thus, this analysis does not constitute a solution to the problem under consideration.

Jeppson [28] proposed an inverse formulation of the problem for the flow exiting from a circular orifice by using x and r as dependent variables and ϕ and ψ as the independent variables. Through the use of this technique Jeppson [29] also analyzed the flow of a jet from a convergent nozzle with curved boundaries.

All of the investigations described so far have attempted to provide better solutions to the various configurations of the orifice flow. These techniques suffer in general from convergence and accuracy problems and nearly all resort to simple trial-and-error procedures to locate the free surfaces and to satisfy the boundary condition that the free surfaces be streamlines of constant velocity. Suffice it to say that

a method was needed which could yield solutions of a prescribed accuracy for a wide variety of fluid flow problems involving Dirichlet, Neumann, and mixed boundary conditions.

Zienkiewicz and Cheung [30] proposed in 1965 the application of the finite element method to the solution of field problems involving the equations of Laplace and Poisson. Since then a significant number of applications of the finite element method to fluid dynamics has appeared in the literature (see e.g. Norrie and de Vries [31] and the references cited therein).

The method has been recently applied to several jet-efflux problems involving only one freestream surface and relatively small jet contraction by Chan and Larock [32]. Suffice it to say that the finite element method has proven its versatility and applicability to a wide variety of two-dimensional and axisymmetric flow-problems. The truly three-dimensional problem such as the oblique impact of a circular jet on a plane surface, with or without gravitational forces, just to name one, offers considerable challenges and demands additional sophistication.

The special case of the gravitational force acting along the axis of symmetry may easily be analyzed by modifying the boundary conditions such that the velocity along the free surface varies according to the Bernoulli theorem.

This part of the investigation encouraged by the advent and the continued success of the finite element method is devoted to a determination of the angle of deflection, the

location of the freestream surfaces and the velocity and pressure distributions caused by a finite curved boundary in general and a hemispherical boundary in particular placed symmetrically with respect to the axis of an axisymmetric, inviscid jet issuing from a nozzle. This problem has not been previously analyzed through either exact or approximate methods.

As stated earlier, the deflection of a jet by a solid boundary is well suited to potential-flow analysis because of the dominance of inertia and pressure forces in the establishment of the flow pattern. The result in general represents asymptotic values which are approached as the effect of secondary variables such as entrainment, boundary layer, compressibility, jet attachment to adjacent surfaces (Coanda effect), etc. are decreased. Specifically, if the total angle through which the jet is deflected is determined for idealized conditions, then the principle of impulse and momentum can be used to compute pressures, forces, or other dynamic characteristics of the system such as the reverse-thrust ratio. In this manner one can not only optimize the geometry of the system for optimum performance, measured in terms of reversed thrust, but also can assess the significance of the real-fluid effects, cited above, on its performance.

B. ANALYSIS

The problem may be defined in general with reference to Figure 10. An axisymmetric jet issues from a nozzle $\overline{BC}$

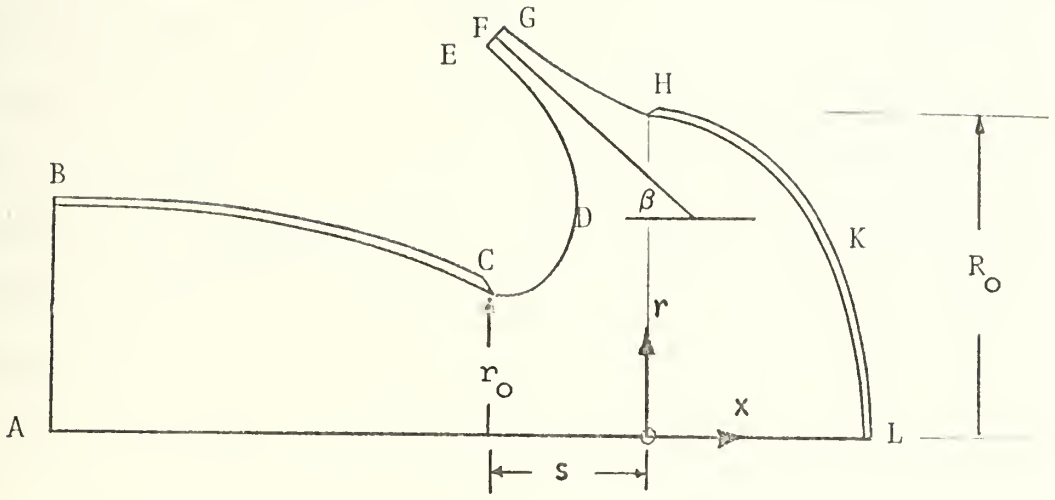

Figure 10 General case of axisymmetric bucket an nozzle

with an entrance velocity V_o at $\overline{AB}$. The jet impinges symmetrically upon the curved bucket $\overline{LKH}$ and then the deflected jet leaves at an angle β. The upper and lower surfaces of the jet; namely, $\overline{CDE}$ and $\overline{HG}$, asymptotically converge to the centerline of the jet in accordance with the conservation of mass.

It is apparent from Fig. 10 that for a given nozzle and bucket shape, the deflection angle varies with the diameters of the bucket and the nozzle and the separation distance between the lips of the nozzle and the bucket. In other words, β can be expressed as

$$\beta = \beta(R_o/r_o \ , \ s/r_o) \tag{56}$$

Thus, the determination of this functional relationship constitutes the basis of the problem.

The fluid is assumed to be inviscid, incompressible, and free from body forces. Consequently, the problem may be formulated in terms of either the velocity potential ϕ or the Stokes stream function ψ. Here the potential function is chosen as the unknown field parameter.

The governing equation is then given by

$$\frac{\partial^2\phi}{\partial x^2} + \frac{1}{r}\frac{\partial\phi}{\partial r} + \frac{\partial^2\phi}{\partial r^2} = 0 \tag{57}$$

in which x and r are the axial and radial coordinates. Because of the axial symmetry there is no variation in the meridional direction. This equation is to be solved with the boundary conditions which simply states that the normal component of velocity be zero along both the solid and free surfaces, i.e. the free surfaces be streamlines of constant velocity.

For an axisymmetric flow, the solution to the Laplace-field equation satisfying the specified normal-velocity boundary condition $(\partial\phi/\partial n)^a$ is given by the admissible function ϕ which minimizes the functional (see e.g. Zienkiewicz and Cheung [30])

$$I(\phi) = \rho\pi \iint_A [(\frac{\partial\phi}{\partial x})^2 + (\frac{\partial\phi}{\partial r})^2]rdxdr - 2\rho\pi \oint_C \phi(\frac{\partial\phi}{\partial n})^a \, rdS \tag{58}$$

in which A is the half of a meridional section of the flow and C is a portion of the curve bounding this area where the normal derivatives are prescribed. The first integral in Eq. (58) represents the kinetic energy of the fluid within the entire control volume and the second integral represents twice the work done by the impulsive pressure $\rho\phi$ on the boundaries in starting the motion from rest (Milne-Thompson [4]).

It is apparent from the foregoing that in the finite-element method the boundary conditions are an integral part of the functional $I(\phi)$ and will not have to be dealt with separately as in the case of finite-difference or relaxation techniques. This is, in fact, where the beauty and the power of the finite element technique lie.

The approximate minimization of the functional $I(\phi)$ is accomplished as follows. Firstly, the field of interest is divided into M triangular elements and a functional $I(\phi)$ is written as a sum of M element-functionals $I^e(\phi)$ each of which has the form of Eq. (58), i.e.

$$I(\phi) = \sum_{1}^{M} I^e(\phi) \qquad (59)$$

Figure 11 shows the numbering system of the corners and mid-points and the corresponding area coordinates $\zeta_i = A_i/A^e$ in which A_i is the area of a subtriangle and A^e is the area of the entire triangle. Then it is clear that $\zeta_1 + \zeta_2 + \zeta_3 = 1$.

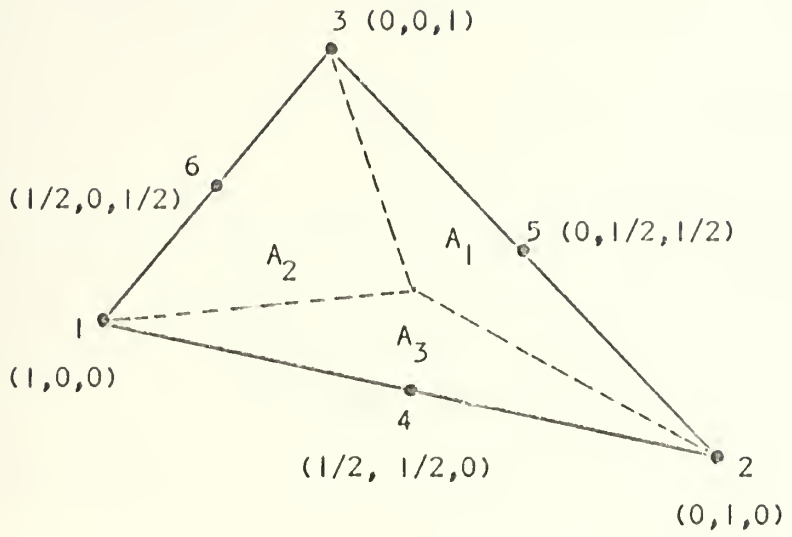

Figure 11 A triangular element with area coordinates

Secondly, a polynomial of sufficient order is selected to represent the variation of the potential function ϕ^e within each element.

Apparently, a linear variation of ϕ^e leads to constant velocities along a given line within an element and to unacceptably large errors in the velocities between neighboring elements. A second-order polynomial, however, allows at least a linear variation of velocity components.

The use of higher order polynomials may increase the accuracy of the results and the convergence of the minimization, but it may also lead to extremely tedious arithmetical manipulations. For these reasons and following Felippa [33] and

Chan and Larock [32], a second-order polynomial has been chosen. In terms of the area coordinates, this leads to

$$\phi^e = \phi_i^e \chi_i \quad (i = 1, \ldots, 6) \tag{60}$$

where ϕ_i^e are the coefficients of the polynomial and corresponds to the values of ϕ^e at the node i. It is important to note that ϕ_i^e must be regarded as constants during the integration of Eq. (58) in each element.

The term χ_i may be written after Felippa [33] as

$$\chi_i = [\zeta_1(2\zeta_1-1), \zeta_2(2\zeta_2-1), \zeta_3(2\zeta_3-1), 4\zeta_1\zeta_2, 4\zeta_2\zeta_3, 4\zeta_1\zeta_3] \tag{61}$$

The velocity components u and v are given by

$$u = \frac{\partial \phi}{\partial x}$$

and

$$v = \frac{\partial \phi}{\partial r}$$

Then the velocity in each element can be written as

$$u^e = \phi_i^e \frac{\partial \chi_i}{\partial x} \quad (i = 1 \text{ to } 6) \tag{62}$$

$$v^e = \phi_i^e \frac{\partial \chi_i}{\partial r} \quad (i = 1 \text{ to } 6) \tag{63}$$

The evaluation of Eqs. (62) and (63) require the derivatives of χ_i with respect to x and r or the evaluation of terms such as

$$\frac{\partial[\zeta_1(2\zeta_1-1)]}{\partial x} = (4\zeta_1-1)\frac{\partial \zeta_1}{\partial x} = (4\zeta_1-1)\frac{b_1}{2A^e} = T_1^e$$

$$\frac{\partial[\zeta_2(2\zeta_2-1)]}{\partial x} = (4\zeta_2-1)\frac{\partial \zeta_2}{\partial x} = (4\zeta_2-1)\frac{b_2}{2A^e} = T_2^e$$

$$\frac{\partial[\zeta_3(2\zeta_3-1)]}{\partial x} = (4\zeta_3-1)\frac{\partial \zeta_3}{\partial x} = (4\zeta_3-1)\frac{b_3}{2A^e} = T_3^e$$

(64)

$$\frac{\partial(4\zeta_1\zeta_2)}{\partial x} = 4\zeta_1\frac{\partial \zeta_2}{\partial x} + 4\zeta_2\frac{\partial \zeta_1}{\partial x} = \frac{4}{2A^e}(\zeta_1 b_2 + \zeta_2 b_1) = T_4^e$$

$$\frac{\partial(4\zeta_2\zeta_3)}{\partial x} = 4\zeta_2\frac{\partial \zeta_3}{\partial x} + 4\zeta_3\frac{\partial \zeta_2}{\partial x} = \frac{4}{2A^e}(\zeta_2 b_3 + \zeta_3 b_2) = T_5^e$$

$$\frac{\partial(4\zeta_1\zeta_3)}{\partial x} = 4\zeta_1\frac{\partial \zeta_3}{\partial x} + 4\zeta_3\frac{\partial \zeta_1}{\partial x} = \frac{4}{2A^e}(\zeta_1 b_3 + \zeta_3 b_1) = T_6^e$$

in which

$$\frac{\partial \zeta_i}{\partial x} = \frac{b_i}{2A^e}$$

and

$$b_k = r_i - r_j$$

The foregoing closely follows the notations developed by Felippa [33].

It is evident that the derivatives of χ with respect to r may easily be evaluated by changing x to r or b_i to a_i given by

$$a_k = x_j - x_i$$

and denoting the resulting array of T_i by $\tilde{T}_i$. Thus, one can write

$$T_i^e = \frac{(4\zeta_i - 1)b_i}{2A^e} \qquad \text{(no sum on i)} \qquad (65a)$$

$$T_{i+3}^e = \frac{4(b_i\zeta_j + b_j\zeta_i)}{2A^e} \qquad (65b)$$

and likewise

$$\tilde{T}_i^e = \frac{4(\zeta_i - 1)a_i}{2A^e} \qquad \text{(no sum on i)} \qquad (66a)$$

$$\tilde{T}_{i+3}^e = \frac{4(a_i\zeta_j + a_j\zeta_i)}{2A^e} \qquad (66b)$$

In which

$$\frac{a_i}{2A^e} = \frac{\partial \zeta_i}{\partial r}$$

and

$$r = r_1\zeta_1 + r_2\zeta_2 + r_3\zeta_3$$

The minimization of the functional $I(\phi)$ in accordance with the Ritz method requires that the partial derivatives of $I(\phi)$ with respect to ϕ_i be zero. In other words

$$\frac{\partial I^e(\phi)}{\partial \phi_i} = 0 \tag{67}$$

which may be evaluated in a manner quite similar to that used in Eq. (64). Thus, Eq. (67) reduces to

$$\frac{\partial I^e(\phi)}{\partial \phi_i^e} = 2\rho\pi \iint_{A^e} (T_i^e T_j^e + \tilde{T}_i^e \tilde{T}_j^e)\phi_j^e r dA - 2\pi\rho \oint_C \chi_i \left(\frac{\partial \phi}{\partial n}\right)^a r dS = 0 \tag{68}$$

or to

$$\frac{\partial I^e(\phi)}{\partial \phi_i^e} = K_{ij}^e \phi_j^e - B_i^e = 0 \tag{69}$$

in which K_{ij}^e and B_i^e represent, respectively, in the structural-mechanics terminology, the element stiffness matrix and the load matrix for a triangular element. In fluid mechanics terminology, they simply represent the geometrical configuration of the grid within the domain and the boundary conditions imposed on it. These coefficients have been previously obtained by Chan and Larock [32] and are tabulated in Appendix G.

In fluid-flow problems where one or more parts of the boundary are to be determined as part of the numerical analysis, the solution of the system of equations represented

by Eq. (69) through the use of the Gaussian elimination procedure requires the use of a suitable (i.e. accurate and convergent) iteration scheme. This important phase of the analysis will be described in the following.

C. ITERATION SCHEME

The iteration scheme consists of the designation of a moving and fixed grid, the adoption of a scheme for assuming the initial position of the deflected jet, and the successive adjustment of the free surfaces until the boundary conditions are satisfied.

1. Designation of a Grid

Evidently, the minimization process cannot be carried out with a fixed grid as it would be in a structural system subjected to small deformations, primarily because the initial position of the free surface is not a priori known, and the initially-assumed boundaries may be too far off from their final positions. In view of the foregoing, the fluid domain was divided into a moving and a fixed grid (see Fig. 12). The fixed grid occupies that region of the flow which is not, in the final analysis, to be intersected by the free surfaces. This does not impose any restrictions on the analysis and requires no more than a passing familiarity with the elementary principles of jet deflection from solid boundaries. Should the boundary of the fixed grid be intersected by the free surface during the iteration process, a new fixed grid has to be assigned.

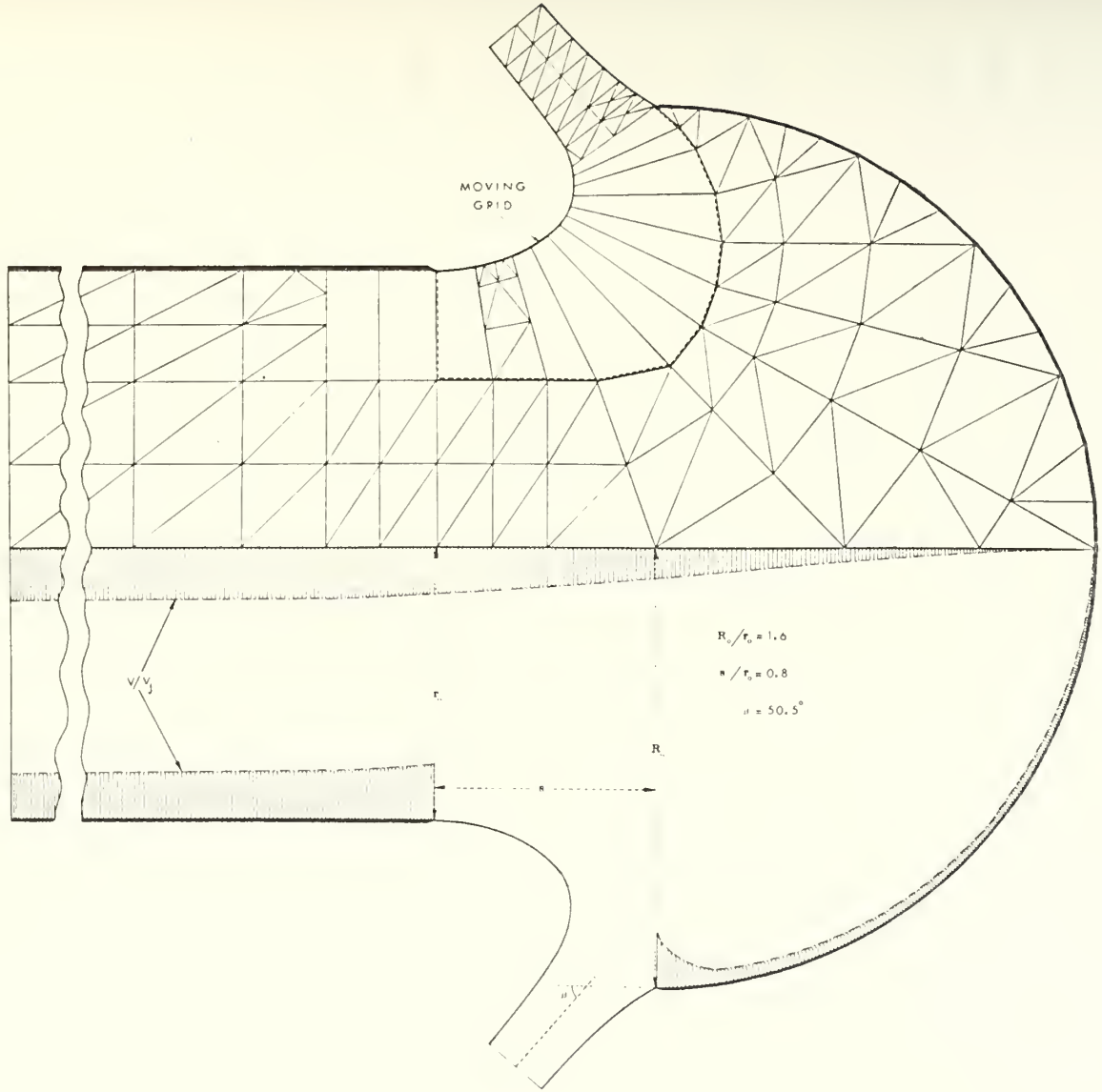

Figure 12 Jet deflection from a hemispherical bucket ($R_o/r_o = 1.6$, $s/r_o = 0.8$)

The moving grid is comprised of triangular elements whose nodal points may be moved along prescribed lines prior to the commencement of the next iteration. This procedure may best be described with reference to Fig. 13. At the end of a given iteration, the nodal points A, B, C are moved inward or outward, in a manner and magnitude to be described later and the positions of the nodal points F, G, E, H, D, and K are recalculated such that

$$\overline{AF} = 0.15\ \overline{AN}$$

and

$$\overline{AG} = 0.50\ \overline{AN}$$

and similarly for $\overline{BE}$, $\overline{BH}$, etc. Evidently, the coefficients 0.15 and 0.50 are arbitrary and different values could have been used provided that the resulting elements maintain a shape more or less compatible to their original shape and that the ratio of the sides of a given element does not significantly differ from unity.

The points intermediate to $\overline{AB}$ and $\overline{BC}$, i.e. the points 1 through 6, are calculated at each iteration through the use of a subroutine called CURVE-FIT. This subroutine is a third order polynomial connecting the points A, B and C, and evenly spacing the points 1 through 3 between $\overline{AB}$ and the points 4 through 6 between $\overline{BC}$. It should be immediately pointed out that there is no need for an exotic subroutine to perform this procedure and that any other judiciously-selected

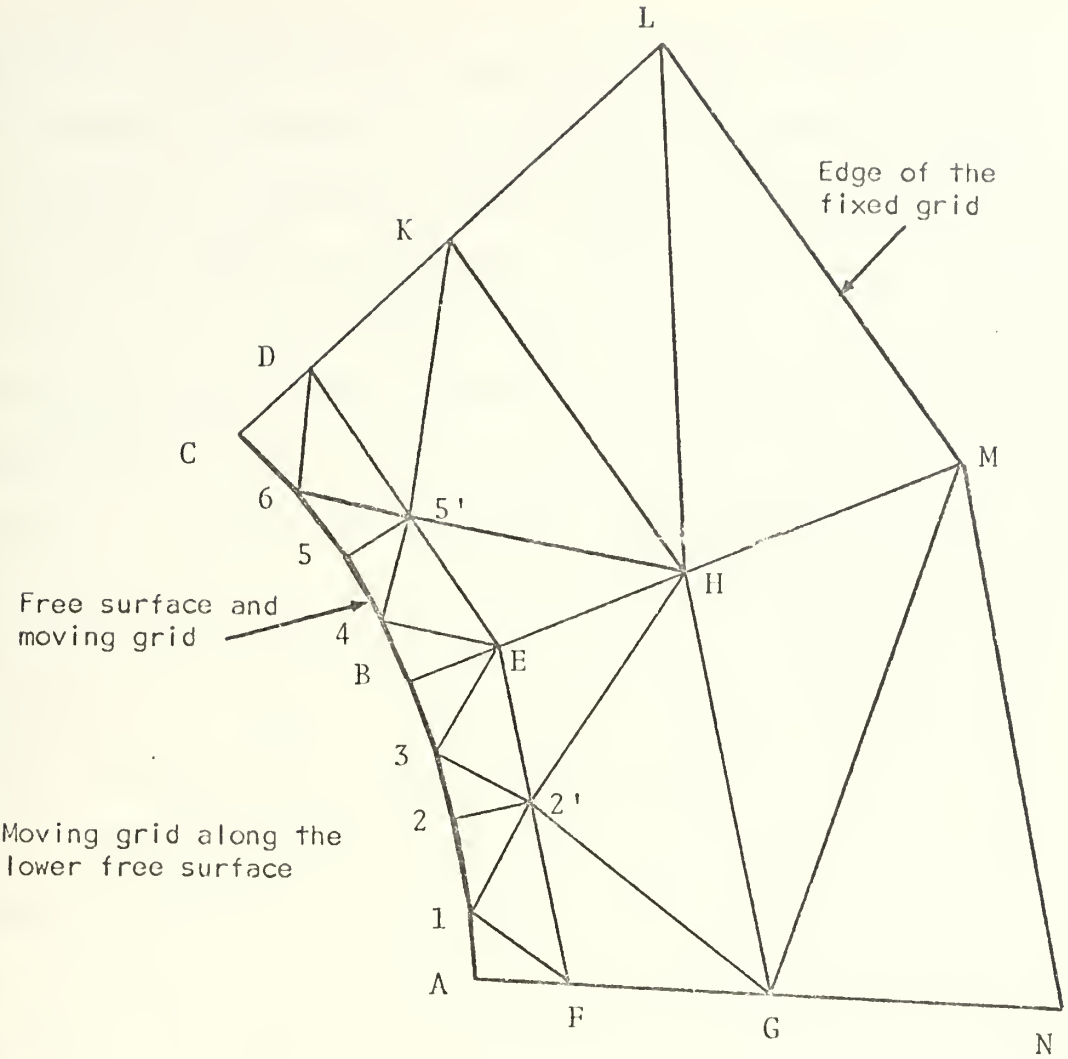

(a) Moving grid along the lower free surface

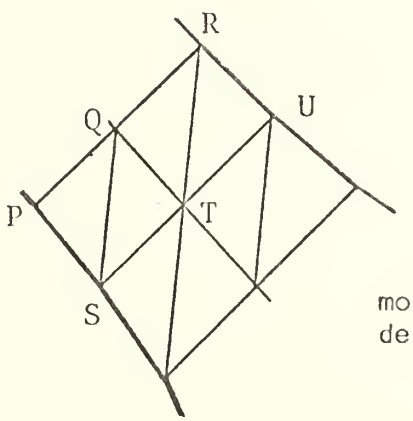

(b) Moving grid in the deflected jet

Figure 13 Construction of the moving grid

polynomial could have been employed. The sole purpose of the foregoing procedure is to smooth the boundary between two successive iterations and to obtain a better representation of the curved streamlines. Furthermore, this procedure eliminates the occurrence of localized low or high velocities which could have stemmed from a zig-zag positioning of the points such as 1, 2, 3 and thereby accelerates the convergence process. In the deflected portion of the free jet (see Fig. 13b) the points such as P and R are moved inward or outward as dictated by the iteration conditions and the point Q is located in the middle of PR prior to each new iteration.

2. Assumption of Initial Boundaries

The assumption of an initial boundary requires the consideration of the equation of continuity, some familiarity with jet deflection problems in fluid mechanics, and possibly the use of a deflection-angle predictor, if one is available.

Ordinarily, a deflection angle β and the length of the deflected free jet ($\overline{HG}$) are assumed (see Fig. 14). Then, through the use of V_o, r_o, r_F, and the equation of continuity, the thickness d of the jet is calcuated, to a first order of approximation by

$$d = \frac{V_o r_o^2}{2r_F} \tag{70}$$

Subsequently, the points G and E are located such that F is intermediate to both. Then the point G is connected to H (the upper lip of the jet) by a straight line, and the point E is smoothly joined to the lower portion of the assumed

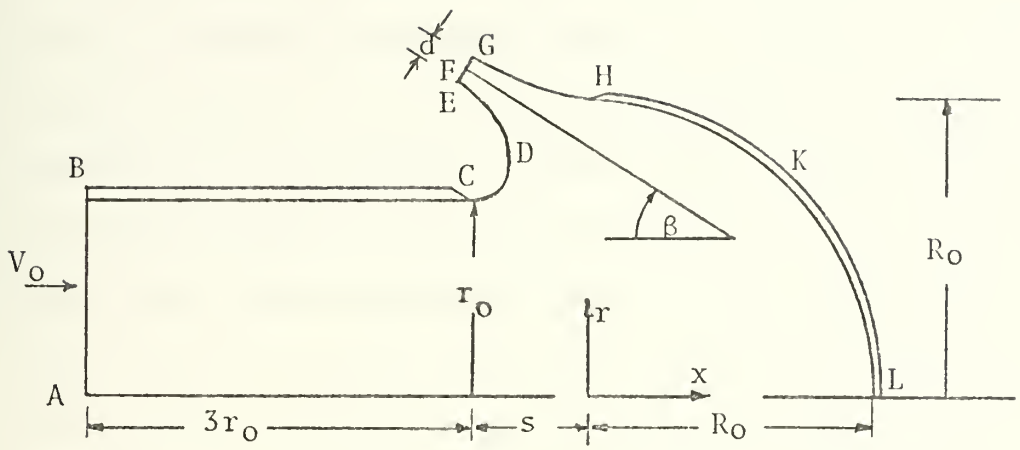

Figure 14 Nomenclature for a hemispherical bucket and straight-nozzle combination

boundary. In passing, it should be noted that the approximate use of the equation of continuity in sections intermediate to $\overline{GH}$ and $\overline{ED}$ may significantly simplify the assignment of the initial position of $\overline{ED}$. For this purpose, all one has to do is to assume a uniform velocity at each section and calculate the thickness of the jet at the section under consideration through the use of an expression similar to that given by Eq. (70).

The description of the assignment of the fluid domain will not be complete without a brief discussion of the length of the nozzle and the deflected jet. Clearly, the sections $\overline{AB}$ and $\overline{EG}$ must be so located that one can for all intents and

purposes assume the velocities at the said sections to be uniform. Otherwise, the analysis will not be correct and the jet boundary will be influenced by the conditions created by the proximity of either the section $\overline{AB}$ and/or $\overline{EG}$ to the points C and H. To this end, preliminary calculations were carried out with nozzle lengths ($\overline{BC}$) as large as $6r_o$ and it was found that it could easily be reduced to $3r_o$ without materially affecting the accuracy of the velocity at $\overline{AB}$. In fact, the calculated velocities at $\overline{AB}$ with a nozzle length of $3r_o$ were accurate within ± 0.5%. Calculations were performed with a nozzle length of $3.8r_o$, i.e. about twice the bucket diameter.

The deflected-jet length $\overline{GH}$ was varied between $0.5r_o$ and $0.7r_o$ depending more or less on the particular angle of deflection. Suffice it to say that no noticeable change was observed in the calculated position of the jet. This is primarily because of the fact that for a jet length of $0.6r_o$, the ratio of the jet length to final jet thickness is about 3.0 and that according to all the previous calculations and exact solutions performed for two- and three-dimensional jets, the jet attains its asymptotic uniform velocity profile in a distance less than 3d.

3. Iteration of the Boundaries

In the foregoing, all of the necessary elements of the analysis and the domain have been provided for the commencement of the iteration process. We will now describe

the process which eventually leads to the final position of the jet for a given geometrical positioning of a hemispherical bucket and a straight nozzle (see Fig. 14).

To begin with, the free surfaces were assumed to be solid boundaries. Thus, the two boundary conditions; namely, constant pressure and zero normal velocity along the free surfaces, reduces to a single condition. Specifically, the freestream surfaces should be streamlines of constant velocity. The normal velocity was written zero everywhere along all the rigid and free surfaces except along $\overline{EG}$ (see Fig. 14). An arbitrary value of $\phi = 100$ was assigned along $\overline{EG}$. Needless to say, the final solution does not depend on this particular value of ϕ.

To start a computation the velocity V_o along $\overline{AB}$ was assumed to be equal to unity and the velocity V_c was calculated. For an exact solution V_c should be equal to unity assuming that the velocities along all the free surfaces are taken equal to unity. Evidently, V_c will turn out to be larger than unity because of the fact that the pressure along $\overline{AB}$ is larger than zero and thus the fluid accelerates along $\overline{BC}$ and decelerates along $\overline{AL}$. The velocity at C was immediately corrected to a first order of approximation by iterating on V_o through the use of the following FORTRAN STATEMENT:

$$V\emptyset = V\emptyset - (VC - 1.0) * V\emptyset \qquad (71)$$

This process of iteration has been used in all subsequent iterations. Apparently, the iteration on V_o could have been accelerated by beginning the analysis with a V_o value smaller than unity (say, $V_o = 0.9$).

Subsequently, the velocities along the free boundaries were calculated everywhere through the use of the ϕ values at the nodal points on the free surface and, as anticipated, it was found that they were not everywhere equal to unity. The reduction of these velocities to unity within a prescribed error constitutes the essence of the iteration process and the use of the moving grid system.

Let V_s represent the velocity at a point along the free surfaces. Then, the free surface at that point was moved inward or outward, depending on whether V_s was greater or smaller than unity, by an amount given by the following statement:

```
DELV = (VS ** 3 - 1.0) * FAC                    (72)
```

in which FAC is a multiplier. The correction DELV was applied to the nodal points along a line normal or nearly normal to the boundary. Various values of FAC have been used in the preliminary calculations, and it was found that a FAC value smaller than 0.05 will yield a convergent iteration. In the present analysis either one of the following two techniques have been used in correcting the free surface. In the first method a single FAC multiplier of 0.015 was applied to both

the upper and the lower boundary, five iterations were performed, and then the angle of deflection β was increased or decreased by two degrees depending on whether the velocities on the upper free surface was smaller or larger than unity. This process has been continued until everywhere the velocities reached a value of 1 ± 0.01. It is important to note that the angle of deflection, the jet thickness, and the radial coordinate r_E and r_G change during each iteration primarily because of the corrections made on the free surfaces. However, the change in β per iteration was about 0.25 degrees. Consequently, one would have needed at least 40 iterations to reach a correct jet position from an initially assumed position with an error of ± 10°. Evidently, then, the ± 2° increments applied to β have accelerated the convergence process.

In the second method two FAC values were used; namely, FACU = 0.001 and FACL = 0.015. Five iterations were carried out by applying FACU to the upper portion of the jet (along $\overline{GH}$ in Fig. 14) and FACL was applied to the lower boundary. At the end of the fifth iteration the role of the FAC values were interchanged and five more iterations were carried out. This simply amounted to first iterating on the lower boundary and then on the upper boundary. As before, the deflection angle was incremented by two degrees until the correct jet deflection angle has been arrived at, as evidenced by the uniformity of the velocities along the upper and lower free surfaces.

The full description of the iteration process would not be complete without stressing few other computational procedures which have enabled the prediction of the initial deflection angle and signaled at the arrival of the correct jet position. These will now be described.

The boundaries were iterated upon through the use of either one of the two methods cited above until a deflection angle has been arrived at which was not more than a few degrees off from the final jet position. At that time no limitations were imposed on the number of iterations and the jet was allowed to arrive at its final position. In passing, it should be noted that the programs were written in FORTRAN IV and double precision arithmetic was used. Since the programs on the Naval Postgraduate School computer (IBM 360-67) had to be run overnight for a period of about one hour, the stops between two successive runs have provided the writer with an opportunity to examine the variation of the velocities, to observe the speed of convergence and finally to decide as to whether one has arrived at the stage of letting the computer finally carry out twenty to twenty-five iterations to establish the final jet position.

Ordinarily, in dealing with the analysis of jet deflection problems from arbitrarily-shaped curved surfaces, one will have at first very little insight as to the value of the deflection angle which the jet will finally assume. However, after one or two calculations with one or two geometrical combinations of a given bucket and nozzle shape,

one will not only be able to guess fairly accurately the initial jet-deflection angle but will also be able to derive a predictor equation. We will now describe the derivation of such an approximate equation which has been useful in predicting an initial deflection angle for all the remaining cases following the study of the first case.

Consider the equation of momentum applied to the fluid domain under consideration:

$$P_o \pi r_o^2 + \pi r_o^2 \rho V_o^2 + \pi r_o^2 \rho V_o V_j \cos \beta = T \qquad (73)$$

in which P_o represents the uniform pressure along $\overline{AB}$, V_j the velocity along the free streamlines ($V_j = 1$ in the present analysis), ρ the density of fluid, and T the force required to hold the bucket at rest. Evidently, if V_o, β, and V_j were known, then the force acting on the bucket could have been calculated. In fact, the present analysis does enable one to do so not only through the use of the momentum equation but also through the integration of P dA (dA is the projected elemental area of the bucket at the center of which the pressure is P). Since the velocities along the bucket were known for the first case, P dA was integrated and the resulting thrust was calculated. This procedure has not only provided a means of checking the thrust calculated from the momentum equation, but also an equation to predict the deflection angle for other geometrical combinations of the nozzle and the bucket. Thus, writing

$$\int PdA = 2\, r_o^2 \left[1 + \left(\frac{V_o}{V_j}\right)^2 + \frac{V_o}{V_j} \cos \beta\right] \qquad (74)$$

one has

$$\cos \beta = \frac{\frac{1}{2} \int PdA - \pi[1 + (V_o/V_j)^2]}{2\pi(V_o/V_j)} \qquad (75)$$

The equations so far derived are exact and Eq. (75) could be used as a mean to predict the angle of deflection for other R_o/r_o and s/r_o values if one assumes that $\int PdA$ remains essentially constant. Thus using the $\int PdA$ value obtained from the first case and a V_o value of approximately 0.8, one arrives at the initial value of β. It should be stressed that the foregoing procedure is designed simply to help the analyst to arrive faster at the correct solution. It neither alters the final result nor is absolutely necessary for the solution of the problems discussed here.

D. HEMISPHERICAL TARGET-TYPE THRUST REVERSERS

The use of thrust reversers on modern jet craft for the purposes of decreasing the landing load, maintaining 100% engine speed while landing, decreasing the thrust while maneuvering, reducing the length of the landing strip, tire wear and tear, etc. has been one of the most important developments in aircraft industry in the last two decades. To perform effectively, a thrust reverser should yield a relatively small jet-deflection angle, should have easy

stowage configuration, should have relatively small boattail or stowage drag, and finally should not adversely affect the engine performance. A hemispherical thrust reverser appears to fulfill these requirements. Furthermore, there exist some experimental data on this type of reverser (Steffen et al. [34] and Povolny et al. [35]) for comparison with the results of the present analysis.

So far as the finite element method is concerned, there is no restriction on the nozzle and the bucket shape and they could be of any axisymmetric, reasonably-chosen configurations. In other words, the finite-element method enables one to optimize, within the assumptions of the inviscid flow theory, the relative position of a given bucket and nozzle, the effect of some geometrical modifications on the bucket and/or nozzle shape (such as placing a flat plate within the bucket) on the performance of the reverser. Furthermore, it enables one to assess the degree of significance of the real-fluid effects such as viscous and turbulent energy dissipation, entrainment, Coanda effect, nozzle-pressure ratio, etc. on the actual performance of the bucket.

The geometrical configurations, namely, the ratios R_o/r_o and s/r_o were chosen partly on the basis of the past experience with such reversers. For example, it has been experimentally demonstrated by Steffen et al. [34] that the larger bucket, the larger is the reversed thrust and that the closer the nozzle to the bucket, the larger is the back-pressuring effect. In other words, when a nozzle is placed very close

to the bucket, the pressure rises in the nozzle because of the blockage of the flow by the bucket and this, in turn, tends to affect the engine performance. Therefore, there is an optimum nozzle-bucket configuration which yields optimum reverser performance.

It is on the basis of such considerations that the nozzle-bucket geometries listed in Table I have been chosen for the numerical analysis and experiments.

TABLE I

	Geometrical Charact. of the Hemispherical buckets analyzed		Angle of Deflection β (deg.)			
			Finite element analysis			Experimental (water)
Case No.	R_o/r_o	s/r_o	slope of the inner surface	mean deflection angle	slope of the outer surface	slope of the outer surface
1	1.8	0.4	21.1	20.3	19.5	18
2	1.8	0.8	37.0	35.0	33.0	30
3	1.6	0.8	53.2	50.5	47.8	46

The coordinates of the free surfaces for the three cases cited in Table I are presented in Appendix H. The computer program used in the study of the case number 3 is given in Appendix I. Suffice it to say that similar programs were used for the analysis of the other two cases. The minor differences between the three computer programs essentially resulted from the use of different moving and fixed grids to suit the

particular geometry under study. An effort has been made to keep the number of elements and the bandwidth in the resulting matrix as low as possible and yet maintain a reasonable degree of accuracy. At various stages in the evolution of the computer programs larger or smaller number of elements have been used, and it was found that the number of elements used herein (288) is quite sufficient. Needless to say, the coordinates of the free surfaces may be calculated to a greater degree of precision by increasing the number of the elements particularly in the moving grid. The additional corrections to be applied to the nodal points on the free surfaces at the end of the final iteration were less than 10^{-3}. It is estimated that the calculated deflection angle will not vary more than $\pm 1.0°$. In view of the fact that the real-fluid effects such as entrainment, Coanda, etc., can decrease the deflection angle by as much as ten degrees, it was not deemed necessary to pursue the calculation of the deflection angle to a greater degree of precision.

A series of experiments were conducted with water through the use of straight, sharp-edged nozzles of appropriate dimensions (see Table I) with a hemispherical cup of 0.72 inch radius primarily for the purpose of determining the slope of the outer surface of the deflected jet. The slope was determined from photographs similar to that shown in Fig. 15 and tabulated in column 7 of Table I.

It is evident from Table I that the experimentally determined values of β are somewhat smaller than those obtained

Figure 15 Water jet deflected by a hemispherical bucket
($R_o/r_o = 1.6$, $s/r_o = 0.8$)

numerically (see columns 6 and 7, Table I). The reasons for these differences are several, the most notable ones being the energy dissipation due to viscous action and the Coanda effect. The latter will be discussed in detail further later in connection with the experiments conducted with air. Suffice it to say that the Coanda effect with water is relatively small and the difference between the computed and the measured angles of deflection is within the range of experimental errors and numerical approximations.

The theoretical and experimental results may also be compared in terms of a measure of the reversed-thrust because of its obvious practical significance.

In the aircraft industry the performance of the reverser is expressed in terms of a reverse-thrust-ratio η_R defined by

$$\eta_R = \frac{\text{actual reversed thrust}}{\text{forward thrust of the nozzle alone}}$$

or in other words by

$$\eta_R = \frac{\pi r_o^2 \rho V_j V_o \cos \beta}{\pi r_o^2 \rho V_j^2} = \frac{V_o}{V_j} \cos \beta$$

The η_R values found in the present analysis, and those obtained experimentally by Steffen et al. [34] are tabulated below.

TABLE II

Case No.	η_R Present Analysis	η_R Experimental [34]
1	0.766	0.82
2	0.725	0.79
3	0.515	0.62

Evidently the η_R values obtained experimentally by Steffen et al. [34] are somewhat larger than those obtained in the present analysis. As noted earlier, the observed differences are primarily due to the Coanda effect and the nozzle-pressure ratio. The Coanda effect decreases the deflection angle and thereby increases the reversed thrust. In the experiments conducted by Steffen et al. [34] the outer surface of the nozzle was streamlined in the form of a boattail to decrease entrainment and thus to decrease β or to increase η_R. In fact, as noted by Steffen et al. [34], the pressure reductions on the boattail were large enough to account for as much as 10 to 15 degrees reduction in the deflection angle. Thus the relatively large differences between the η_R values computed in the present analysis and those obtained by Steffen et al. [34] are primarily attributable to the Coanda effect.

In order to illustrate the influence of the Coanda effect, one particular experiment was carried out with air using a 1.25 inch radius nozzle and a 2 inch radius hemispherical bucket with a 1 inch spacing (i.e. with $R_o/r_o = 1.6$ and $s/r_o = 0.8$). The photograph of the deflected jet (visualized with aluminum powder) is shown in Fig. 16a. Figure 16b shows the deflection of a water jet from a similar nozzle-bucket geometry. It is evident from the comparison of these two photographs that whereas the slope of the outer free surface with air is 33 degrees, with water it is 46 degrees. The 13 degree reduction in the deflection angle due to the Coanda effect corresponds to an approximately 20% reduction in η_R. This brings the calculated η_R values into closer agreement with those experimentally obtained.

The nozzle-pressure ratio (total nozzle pressure/ambient pressure) or the actual velocity in the nozzle causes variations in β primarily because the entrainment needs of the deflected jet and hence the Coanda effect increases with increasing jet velocity.

Suffice it to say that the analysis of thrust reversers is extremely complex for the cases where the jet impinges asymmetrically or where the gravitational effects are important. Furthermore, some of the practical problems associated with thrust reversal, such as the reattachment of the jet to the nacelle of the engine, hot gas reingestion, interaction of the deflected jet with the ambient stream and the adjacent surfaces (in this case the outer surface of the nozzle) cannot

(a) Air jet

(b) Water jet

Figure 16 Air and water jets deflected by a hemispherical bucket ($R_o/r_o = 1.6$, $s/r_o = 0.8$)

yet be analyzed by any one of the existing numerical methods, even for relatively simple two-dimensional geometries composed of straight boundaries. Entrainment depends on the velocity distribution and the turbulence level in the jet, shape of the adjacent surfaces, the physical properties of the jet and of the fluid medium into which the jet discharges. Most of these parameters are obviously interdependent and at present there does not seem to be any hope that their effect on the deflection of an axisymmetric jet can be evaluated.

Nevertheless, approximate analyses such as the one presented herein help to isolate the more promising types of thrust reversers, investigate their potentialities, evaluate their ideal performance characteristics, and to delineate the range of importance of the geometrical variables involved. Then those cases that are shown to be promising through computer experiments can be tested in a laboratory, at a sufficiently reduced expense, to evaluate the effect of additional fluid-mechanical phenomena on their actual performance.

IV. SUMMARY OF RESULTS AND CONCLUSIONS

A class of analytical and numerical solutions to the problem of inviscid-jet deflection from plane and axisymmetric concave surfaces have been presented. The methods of solution for the two-dimensional cases included the modified-hodograph method developed herein as well as those devised by Levi-Civita and Riemann and Hilbert.

The modified-hodograph method is capable, within the limitations of the potential-flow theory, of analyzing the flow in curved obstacles and generating a family of practically suitable bucket shapes. Furthermore, this method has the inherent capability of being extended to the generation of even a larger family of concave-obstacle shapes through the use of distributed sources and sinks in the hodograph-plane.

The method devised by Levi-Civita and successfully extended and employed herein requires the judicious selection of the variation of two parameters and the use of a suitable series (such as the Fourier series) to enable one to perform the integrals leading to the coordinates of the obstacle as well as of the free surfaces. A brief familiarity with this method allows one not only to generate a family of suitable concave obstacles but also to round the corners of a bucket composed of straight segments. This procedure has been illustrated by rounding the corners of a U-shaped obstacle previously analyzed by Sarpkaya [1].

As to the Riemann-Hilbert mehtod, it has been demonstrated that it is in essence a mathematically more elegant and sophisticated version of Levi-Civita's method in prescribing certain functions. It is for this reason that no particular solutions have been presented and only a linear variation of the parametric function was discussed.

These methods have provided indirect solutions for the shape of the curved solid boundary in terms of a given jet-departure and jet-deflection angle. The direct solution of the corresponding problems requires the use of either a sequence of iterations or a numerical scheme for solving the Laplace-field problem. The latter method has been reserved for the analysis of the axisymmetric cases because of their far reaching and relative practical significance.

The axisymmetric cases, namely, the deflection of a jet issuing from a nozzle from hemispherical thrust reversers have been solved directly through the use of the finite element method. In doing so, several new procedures have been introduced. These include the use of a self-adjusting and fixed grid and a convergent iteration scheme. The jet-deflection angle, the slope of the inner and outer surfaces of the deflected jet as well as the coordinates of the free streamlines were determined for a series of representative nozzle-hemisphere combinations. It has been demonstrated that the method and the iteration scheme are sufficiently general to analyze the more promising types of thrust-reversers, evaluate their performance characteristics, and to delineate

the range of importance of the geometrical variables involved. Finally, a few experiments have been carried out with air and water to assess the degree of significance of the real-fluid effects on jet deflection. These experiments as well as those conducted by others showed that in cases where the Coanda effect is negligible (water jet in air), the analytically-predicted and experimentally-measured jet-deflection angles are in good agreement and that the real-fluid effects are negligible. This is evidence of the fact that the deflection of a free jet by a solid boundary is well suited to potential flow analysis particularly for the cases where the inertia forces dominate the establishment of the flow pattern. In cases where the Coanda effect is not negligible (air jet in air), the real-fluid effects are more pronounced and can cause the deflection angle to be as much as 20% lower than those predicted from the potential-flow theory. Nevertheless, the potential-flow analysis of the two-dimensional as well as axisymmetric jet-deflection problems enables one to determine the optimum values of the geometrical variables involved and thereby eliminates the use of costly trial and error techniques. With such information available, the real-fluid effects could be evaluated with a few carefully chosen experiments and the refinements of design could be based upon a secure knowledge of the known principles of hydrodynamics.

```
C**********************************************************************
C**                                                                  **
C**                        APPENDIX A                                **
C**                                                                  **
C** COORDINATES OF THE BUCKET FOR K=.001186 CORRESPONDING            **
C**              TO A DEFLECTION ANGLE BETA=50.0 DEG.                **
C**                                                                  **
C**********************************************************************
```

X=0.0505	Y=0.7916
X=0.1002	Y=1.1097
X=0.1531	Y=1.3654
X=0.2025	Y=1.5637
X=0.2577	Y=1.7553
X=0.3033	Y=1.8970
X=0.3503	Y=2.0305
X=0.4008	Y=2.1626
X=0.4511	Y=2.2845
X=0.5020	Y=2.3996
X=0.5505	Y=2.5025
X=0.6026	Y=2.6070
X=0.6539	Y=2.7041
X=0.7061	Y=2.7979
X=0.7513	Y=2.8753
X=0.8048	Y=2.9629
X=0.8525	Y=3.0377
X=0.9095	Y=3.1229
X=0.9545	Y=3.1875
X=1.0073	Y=3.2606
X=1.0541	Y=3.3226
X=1.1092	Y=3.3931
X=1.1523	Y=3.4463
X=1.2024	Y=3.5059
X=1.2622	Y=3.5742
X=1.3362	Y=3.6546
X=1.3809	Y=3.7011
X=1.4332	Y=3.7533
X=1.4958	Y=3.8128
X=1.5741	Y=3.8823
X=1.6783	Y=3.9634

```
C**********************************************************************
C*                                                                    **
C*                  APPENDIX B                                        **
C*                                                                    **
C*        MODIFIED HODOGRAPH METHOD                                   **
C*                                                                    **
C*    COMPUTATION OF THE COORDINATES OF THE BUCKET                    **
C*            FOR A GIVEN DEFLECTION ANGLE BETA                       **
C*                                                                    **
C**********************************************************************
C
      IMPLICIT REAL*8(A-H,O-Z)
      PI=3.14159260D0
      OPI=1.0/PI
      BETA=0.0
      BETA=20.0
C
C    EVALUATE THE BUCKET COORDINATES EACH 10 DEGREES OF BETA
C
      DO 1 I=1,7
      BETA=BETA+10.0
      BE=BETA*PI/180.0
C
C    EVALUATE THE PARAMETER K (XK) FROM EQ.(17)
C
      XK=DEXP(-PI*DSIN(BE)/(1.0-DCOS(BE)))
      WRITE(6,10)
      WRITE(6,11) BETA,XK
   10 FORMAT(5X,'.................',/)
   11 FORMAT(5X,'DEFLEC. ANGL. BETA=',F5.2,'PARAM.K=',F12.10
     8,/)
C
C    DEFINE XO FROM EQ.(15) AND VARY T FROM -1 TO 0
C
      XC=OPI* DLOG((1.0+XK)**2/(4.0*XK))
      T= 1.00001D0
      DT=0.0001D0
      Y=0.0
      DO 2 J=1,10000
      T=T-DT
      Y=2.*(1./(T+XK)+1./(T+1./XK)-2./(T+1.))*DT/DLOG(T)+Y
C
C    CALCULATE AND WRITE X AND Y COORDINATES
C
      X=OPI* DLOG((T+XK)*(T+1.0/XK)/(T+1.0)**2)-XC
      WRITE(6,12) X,Y
   12 FORMAT(5X,'X=',F8.3,3X,'Y=',F8.3)
    2 CONTINUE
    1 CONTINUE
      STOP
      END
```

APPENDIX C

EVALUATION OF THE COEFFICIENTS OF THE FOURIER SERIES REPRESENTING $\theta(\sigma)$

Let $\theta(\sigma)$ be represented by the series

$$\theta(\sigma) = \sum_{n=0}^{\infty} a_n \cos n\sigma \qquad n = 0,1,2,3,... \qquad \text{(A-1)}$$

According to Fig. 6, $\theta(\sigma)$ is defined by

$$\begin{aligned}
\theta(\sigma) &= -\pi && 0 < \sigma < \sigma_1 \\
\theta(\sigma) &= \frac{\pi}{2}\left(\frac{\sigma}{\sigma_2-\sigma_1} - 2 - \frac{\sigma_1}{\sigma_2-\sigma_1}\right) && \sigma_1 < \sigma < \sigma_2 \\
\theta(\sigma) &= -\frac{\pi}{2} && \sigma_2 < \sigma < \frac{\pi}{2} \\
\theta(\sigma) &= -\frac{\pi}{2} && \frac{\pi}{2} < \sigma < \pi-\sigma_2 \\
\theta(\sigma) &= \frac{\pi}{2}\left(\frac{\sigma}{\sigma_2-\sigma_1} - \frac{\pi-\sigma_1}{\sigma_2-\sigma_1}\right) && \pi-\sigma_2 < \sigma < \pi-\sigma_1 \\
\theta(\sigma) &= 0 && \pi-\sigma_1 < \sigma < \pi
\end{aligned} \qquad \text{(A-2)}$$

Multiplying Eq. (A-1) by $\cos n\sigma$ and integrating over a period one has,

$$\int_{-\pi}^{\pi} \theta(\sigma) \cos n\sigma \, d\sigma = a_n \int_{-\pi}^{\pi} \cos^2 n\sigma \, d\sigma \qquad \text{(A-3)}$$

Now making use of the symmetry, one obtains

$$a_n = \frac{2}{\pi} \int_0^{\pi} \theta(\sigma) \cos n\sigma \, d\sigma \qquad \text{(A-4)}$$

The above equation can be written as the sum of six integrals corresponding to each range defined by Eq. (A-2). Thus, one has,

$$a_n = \frac{2}{\pi}\left\{ \int_0^{\sigma_1} (-\pi)\cos n\sigma \, d\sigma + \int_{\sigma_1}^{\sigma_2} \frac{\pi}{2} \left(\frac{\sigma}{\sigma_2-\sigma_1} - 2 - \frac{\sigma_1}{\sigma_2-\sigma_1}\right) \cos n\sigma \, d\sigma \right.$$

$$+ \int_{\sigma_2}^{\frac{\pi}{2}} (-\tfrac{\pi}{2})\cos n\sigma \, d\sigma + \int_{\frac{\pi}{2}}^{\pi-\sigma_2} (-\tfrac{\pi}{2})\cos n\sigma \, d\sigma$$

$$\left. + \int_{\pi-\sigma_2}^{\pi-\sigma_1} \frac{\pi}{2} \left(\frac{\sigma}{\sigma_2-\sigma_1} - \frac{\pi-\sigma_1}{\sigma_2-\sigma_1}\right) \cos n\sigma \, d\sigma + \int_{\pi-\sigma_1}^{\pi} 0 \cos n\sigma d\sigma \right\}$$

(A-5)

After the integration one obtains,

$$a_n = \frac{1}{n^2(\sigma_2-\sigma_1)} \left[(\cos n\sigma_2 - \cos n\sigma_1) - (-1)^n \cdot (\cos n\sigma_2 - \cos n\sigma_1) \right]$$

(A-6)

for n = 1,2,3,...

or

$$a_n = \frac{2}{n^2(\sigma_2-\sigma_1)} (\cos n\sigma_2 - \cos n\sigma_1)$$

(A-7)

for n = 1,3,5,7

For n = 0, one has

$$a_o = -\frac{\pi}{2} \tag{A-8}$$

as expected from the average value of the function $\theta(\sigma)$.

```
C*************************************************************
C*                                                           **
C*                    APPENDIX D                             **
C*                                                           **
C*              LEVI-CIVITA'S METHOD                         **
C*                                                           **
C*   COMPUTATION OF THE COORDIAATES OF THE BUCKET AND         **
C*   FREE STREAMLINES, AND THE DEFLECTION ANGLE  BETA        **
C*   FOR GIVEN VALUES OF SIGMA1,SIGMA2 AND K                 **
C*                                                           **
C*************************************************************
C
C     READ THE VALUES OF SIGMA1 (S1), SIGMA2 (S2) AND K (XK)
C
      READ(5,1) S1,S2,XK
      WRITE(6,2) S1,S2,XK
    1 FORMAT(3F10.0)
    2 FORMAT(5X,'SIGMA1=',F9.5,4X,'SIGMA2=',F9.5,5X,'K=',F8.
     84)
C
C     MAIN DO-LOOP TO INTEGRATE  EQS.(40),(41) AND (42)
C
      X=0.0
      Y=0.0
      PI=3.1415926
      PI2=PI/2.0
      S=PI2
      DS=S/300.0
      DO 3 I=1,300
      S=S-DS
C
C     LOOP TO EVALUATE THE FUNCTION H(S),EQ.(38)
C
      H=0.0
      DO 4 J=1,2001,2
      T=J
      H=H+(2.0/(S2-S1))*(COS(T*S2)-COS(T*S1))*SIN(T*S)/T**2
    4 CONTINUE
C
C     DEFINE FUNCTIONS OF THE INTEGRAND
C
      F1=2.0*XK*XK*SIN(S)*(1.0+SIN(S))/(1.0-XK*XK*COS(S)**2)
      SMA=PI2*(S-S1)/(S2-S1)
      CA=COS(SMA)
      SA=SIN(SMA)
C
C     SELECT VALUES OF THETA ACCORDING TO EQ.(39)
C
      IF(S.GT.S2) CA=0.0
      IF(S.GT.S2) SA=1.0
      IF(S.LT.S1) CA=1.0
      IF(S.LT.S1) SA=0.0
C
C     INTEGRATE BY SIMPSON'S RULE
C
      X=X+EXP(-H)*F1*CA*DS/PI
      Y=Y+EXP(-H)*F1*SA*DS/PI
      WRITE(6,6) S,X,Y
    6 FORMAT(5X,'SIGMA=',F8.4,5X,'X=',F7.3,3X,'Y=',F7.3)
    3 CONTINUE
C
C     EVALUATION OF THE ANGLE BETA
C
      C=(1.0-SQRT(1.0-XK*XK))
      BETA=-ATAN(2.0*C/(1.0-C*C))
      DO 7 L=1,301,2
      T=L
      BETA=(2./(S2-S1))*(COS(T*S2)-COS(T*S1))*C**L/T**2+BETA
    7 CONTINUE
      BETA=180.0*(1.0+BETA/PI)
      WRITE(6,8)BETA
    8 FORMAT(5X,'BETA=',F10.3)
```

```
C    EVALUATION OF THE COORDENATES OF THE FREE STREAMLINES
C
       IND=0
       R=-0.0001
       DR=C/1000.0
  12   CONTINUE
       X=0.0
       Y=0.0
       DO 11 I=1,1000
       R=R+DR
       F1=(XK*XK*(R*R-1.0/R**2)/(2.0*R))/((XK**2/4.0)*(R+1.0/
      8R)**2-1.0)
C
C    EVALUATE W(R) FROM EQ.(29)
C
       W=-ATAN(2.0*R/(1.0-R*R))
       DO 10 J=1,1001,2
       T=J
       W=W+(2.0/(S2-S1))*(COS(T*S2)-COS(T*S1))*R**J/T**2
  10   CONTINUE
       X=COS(W)*F1*DR/PI+X
       Y=SIN(W)*F1*DR/PI+Y
       WRITE(6,13) R,X,Y
  13   FORMAT(5X,'R=',F10.6,5X,'X=',F9.3,2X,'Y=',F9.3)
  11   CONTINUE
C
C    GO TO 12 TO EVALUATE THE UPPER FREE STREAMLINE
C
       IND=IND+1
       R=1.0001
       DR=(C-1.0)/1000.0
       IF(IND.EQ.1) GO TO 12
       STOP
       END
```

APPENDIX E

EVALUATION OF THE INTEGRAL FOR $\omega(t)$

$$\omega(t) = \frac{\sqrt{-t(t-k)}}{\pi} \int_1^k \frac{-(a+b\eta)}{(\eta-t)\sqrt{-\eta(\eta-k)}}\, d\eta \qquad \text{(E-1)}$$

Noting that

$$\frac{a}{\eta - t} + \frac{b\eta}{\eta - t} = \frac{a + bt}{\eta - t} + b$$

Eq. (E-1) can be written as,

$$\omega(t) = -\frac{\sqrt{-t(t-k)}}{\pi} \left\{ (a+bt) \int_1^k \frac{d\eta}{(\eta-t)\sqrt{-\eta(\eta-k)}} + b \int_1^k \frac{d}{\sqrt{-\eta(\eta-k)}} \right\} \qquad \text{(E-2)}$$

The second integral in Eq. (E-2) is

$$\int_1^k \frac{d\eta}{\sqrt{\eta(k-\eta)}} = \cos^{-1} \frac{2-k}{k} \qquad \text{(E-3)}$$

The first integral in Eq. (E-2) depends on the particular range of t. For $0 < t < k$, one has,

$$\int_1^k \frac{d\eta}{(\eta - t)\sqrt{\eta(k-\eta)}} = \frac{1}{\sqrt{t(k-t)}} \ln \frac{\frac{k}{2}(t+1) - t + \sqrt{k-1}\sqrt{t(k-t)}}{\frac{k}{2}(t-1)}$$

(E-4)

For $t < 0$ and $t > k$ one obtains,

$$\int_1^k \frac{d\eta}{(\eta - t)\sqrt{\eta(k-\eta)}} = -\frac{1}{\sqrt{t(k-t)}} \cos^{-1} \frac{\frac{2t}{k} - t + 1}{t - 1} \qquad \text{(E-5)}$$

Inserting Eqs. (E-3),(E-4) and (E-5) in Eq. (E-2) one finally obtains,

$$\omega(t) = -\frac{a+bt}{\pi} \ln \frac{\frac{k}{2}(t+1) - t + \sqrt{k-1}\sqrt{t(k-t)}}{-\frac{k}{2}(t-1)} - \frac{b}{\pi}\sqrt{t(k-t)} \cos^{-1} \frac{2-k}{k}$$

for $0 < t < k$, and

$$\omega(t) = \frac{i(a+bt)}{\pi} \cos^{-1} \frac{\frac{2t}{k} - t - 1}{t-1} - i\frac{b}{\pi}\sqrt{t(t-k)} \cos^{-1} \frac{2-k}{k}$$

for $t < 0$ and $t > k$.

APPENDIX F

EVALUATION OF THE DEFLECTION ANGLE β FROM EQ. (52)

Letting $t \to \infty$ in Eq. (52) one has

$$\lim_{t\to\infty} \omega(t) = \frac{i}{\pi} \int_1^k \frac{(a + b\eta)}{\sqrt{\eta(k-\eta)}}\, d\eta \qquad \text{(F-1)}$$

and noting that

$$\beta = \pi - \lim_{t\to\infty} i\omega(t) \qquad \text{(F-2)}$$

Eq. (F-1) can be rewritten after some rearrangement as,

$$\beta = \pi + \frac{(a + \frac{bk}{2})}{\pi} \int_1^k \frac{d\eta}{\sqrt{\eta(k-\eta)}} - \frac{b}{\pi}\sqrt{\eta(k-\eta)}\,\Big|_1^k \qquad \text{(F-3)}$$

Evaluating the integrals and applying the limits of integration, one has,

$$\beta = \pi + \frac{1}{\pi}\left[(a + \frac{bk}{2}) \cos^{-1}\frac{2-k}{k} + b\sqrt{k-1} \right] \qquad \text{(F-4)}$$

Finally, replacing the corresponding values of a and b one obtains,

$$\beta = \pi + \frac{1}{2(k-1)}\left[(\frac{3k}{2} - 2) \cos^{-1}\frac{2-k}{k} + \sqrt{k-1} \right]$$

APPENDIX G

LIST OF COEFFICIENTS K^e_{ij} AND B^e_j

$$S_{ij} = (a_i a_j + b_i b_j)/60A^e$$

$$K^e_{11} = 3S_{11}(3r_1 + r_2 + r_3)$$

$$K^e_{12} = K^e_{21} = - S_{12}(2r_1 + 2r_2 + r_3)$$

$$K^e_{13} = K^e_{31} = - S_{13}(2r_1 + r_2 + 2r_3)$$

$$K^e_{14} = K^e_{41} = S_{11}(3r_1 - 2r_2 - r_3) + S_{12}(14r_1 + 3r_2 + 3r_3)$$

$$K^e_{15} = K^e_{51} = S_{12}(3r_1 - r_2 - 2r_3) + S_{13}(3r_1 - 2r_2 - r_3)$$

$$K^e_{16} = K^e_{61} = S_{11}(3r_1 - r_2 - 2r_3) + S_{13}(14r_1 + 3r_2 + 3r_3)$$

$$K^e_{22} = 3S_{22}(r_1 + 3r_2 + r_3)$$

$$K^e_{23} = K^e_{32} = - S_{23}(r_1 + 2r_2 + 2r_3)$$

$$K^e_{24} = K^e_{42} = S_{12}(3r_1 + 14r_2 + 3r_3) + S_{22}(- 2r_1 + 3r_2 - r_3)$$

$$K^e_{25} = K^e_{52} = S_{22}(- r_1 + 3r_2 - 2r_3) + S_{23}(3r_1 + 14r_2 + 3r_3)$$

$$K^e_{26} = K^e_{62} = S_{12}(- r_1 + 3r_2 - 2r_3) + S_{23}(- 2r_1 + 3r_2 - r_3)$$

$$K^e_{33} = 3S_{33}(r_1 + r_2 + 3r_3)$$

$$K^e_{34} = K^e_{43} = S_{13}(- r_1 - 2r_2 + 3r_3) + S_{23}(- 2r_1 - r_2 + 3r_3)$$

$$K^e_{35} = K^e_{53} = S_{23}(3r_1 + 3r_2 + 14r_3) + S_{33}(- r_1 - 2r_2 + 3r_3)$$

$$K^e_{36} = K^e_{63} = S_{13}(3r_1 + 3r_2 + 14r_3) + S_{33}(- 2r_1 - r_2 + 3r_3)$$

$$K^e_{44} = 8[S_{11}(r_1 + 3r_2 + r_3) + S_{12}(2r_1 + 2r_2 + r_3)$$

$$+ S_{22}(3r_1 + r_2 + r_3)]$$

$$K^e_{45} = K^e_{54} = 8S_{13}(r_1 + 3r_2 + r_3) - 4(S_{12}r_1 + S_{22}r_2 + S_{23}r_3)$$

$$K^e_{46} = K^e_{64} = 8S_{23}(3r_1 + r_2 + r_3) - 4(S_{11}r_1 + S_{12}r_2 + S_{13}r_3)$$

$$K^e_{55} = 8[S_{22}(r_1 + r_2 + 3r_3) + S_{23}(r_1 + 2r_2 + 2r_3)$$

$$+ S_{33}(r_1 + 3r_2 + r_3)$$

$$K^e_{56} = K^e_{65} = 8S_{12}(r_1 + r_2 + 3r_3) - 4(S_{13}r_1 + S_{23}r_2 + S_{33}r_3)$$

$$K^e_{66} = 8[S_{11}(r_1 + r_2 + 3r_3) + S_{13}(2r_1 + r_2 + 2r_3)$$

$$+ S_{33}(3r_1 + r_2 + r_3)$$

In the matrix B^e_i terms, ℓ_i = length of side i of a triangular element. Thus

$$B^e_1 = r_1 \left[\left(\frac{\partial\phi}{\partial n}\right)^{a_2} \ell_2 + \left(\frac{\partial\phi}{\partial n}\right)^{a_3} \ell_3 \right] \frac{1}{6}$$

$$B^e_2 = r_2 \left[\left(\frac{\partial\phi}{\partial n}\right)^{a_1} \ell_1 + \left(\frac{\partial\phi}{\partial n}\right)^{a_3} \ell_3 \right] \frac{1}{6}$$

$$B^e_3 = r_3 \left[\left(\frac{\partial\phi}{\partial n}\right)^{a_1} \ell_1 + \left(\frac{\partial\phi}{\partial n}\right)^{a_2} \ell_2 \right] \frac{1}{6}$$

$$B_4^e = (r_1 + r_2)\left(\frac{\partial\phi}{\partial n}\right)^{a_3}\ell_3\ \frac{1}{3}$$

$$B_5^e = (r_2 + r_3)\left(\frac{\partial\phi}{\partial n}\right)^{a_1}\ell_1\ \frac{1}{3}$$

$$B_6^e = (r_3 + r_1)\left(\frac{\partial\phi}{\partial n}\right)^{a_2}\ell_2\ \frac{1}{3}$$

C**********
C**
C**
C**
C**
C**
C**
C**********

APPENDIX H

COORDINATES OF FREE-STREAMLINES

CASE NUMBER ONE

BETA=20.3 DEG
VO=0.817

X=-0.400	R=1.000
X=-0.370	R=1.003
X=-0.325	R=1.009
X=-0.301	R=1.012
X=-0.263	R=1.020
X=-0.230	R=1.030
X=-0.203	R=1.039
X=-0.181	R=1.042
X=-0.138	R=1.060
X=-0.099	R=1.080
X=-0.066	R=1.100
X=-0.038	R=1.118
X=-0.016	R=1.137
X= 0.001	R=1.158
X= 0.018	R=1.176
X= 0.034	R=1.192
X= 0.053	R=1.224
X= 0.063	R=1.258
X= 0.071	R=1.290
X= 0.072	R=1.323
X= 0.072	R=1.340
X= 0.069	R=1.357
X= 0.065	R=1.375
X= 0.059	R=1.392
X= 0.056	R=1.398
X= 0.053	R=1.405
X= 0.050	R=1.412
X= 0.047	R=1.419
X= 0.044	R=1.425
X= 0.040	R=1.431
X= 0.036	R=1.438
X= 0.032	R=1.444
X= 0.028	R=1.450
X= 0.023	R=1.456
X= 0.018	R=1.462
X= 0.013	R=1.468
X= 0.007	R=1.474
X= 0.001	R=1.481
X=-0.006	R=1.488
X=-0.013	R=1.495
X=-0.024	R=1.505
X=-0.036	R=1.514
X=-0.048	R=1.524
X=-0.062	R=1.533
X=-0.078	R=1.544
X=-0.095	R=1.555
X=-0.113	R=1.565
X=-0.131	R=1.576
X=-0.193	R=1.607
X=-0.252	R=1.634
X=-0.328	R=1.669
X=-0.385	R=1.694
X=-0.457	R=1.724
X=-0.530	R=1.753
X=-0.600	R=1.781
X=-0.658	R=1.805

X=-0.014 R=1.805
X=-0.030 R=1.807
X=-0.045 R=1.813
X=-0.061 R=1.815
X=-0.111 R=1.834
X=-0.173 R=1.855
X=-0.252 R=1.884
X=-0.310 R=1.906
X=-0.373 R=1.933
X=-0.457 R=1.959
X=-0.528 R=1.934
X=-0.587 R=2.005

CASE NUMBER TWO

BETA=35.0 DEG
VO=0.885

X=-0.800 R=1.000
X=-0.774 R=1.001
X=-0.748 R=1.003
X=-0.723 R=1.006
X=-0.697 R=1.009
X=-0.663 R=1.013
X=-0.629 R=1.019
X=-0.595 R=1.025
X=-0.561 R=1.030
X=-0.525 R=1.038
X=-0.489 R=1.047
X=-0.453 R=1.057
X=-0.418 R=1.069
X=-0.394 R=1.080
X=-0.370 R=1.089
X=-0.346 R=1.100
X=-0.324 R=1.111
X=-0.301 R=1.125
X=-0.281 R=1.139
X=-0.260 R=1.153
X=-0.241 R=1.168
X=-0.224 R=1.182
X=-0.208 R=1.199
X=-0.194 R=1.216
X=-0.181 R=1.235
X=-0.166 R=1.258
X=-0.155 R=1.282
X=-0.146 R=1.308
X=-0.142 R=1.335
X=-0.140 R=1.358
X=-0.140 R=1.382
X=-0.143 R=1.404
X=-0.149 R=1.425
X=-0.154 R=1.443
X=-0.161 R=1.461
X=-0.168 R=1.478
X=-0.177 R=1.495
X=-0.184 R=1.506
X=-0.191 R=1.517
X=-0.200 R=1.529
X=-0.209 R=1.539
X=-0.243 R=1.579
X=-0.304 R=1.635
X=-0.367 R=1.689
X=-0.430 R=1.733
X=-0.494 R=1.791
X=-0.562 R=1.838

X=-0.000 R=1.800
X=-0.068 R=1.800
X=-0.083 R=1.803
X=-0.137 R=1.809
X=-0.150 R=1.855

X=-0.234 R=1.883
X=-0.288 R=1.947
X=-0.367 R=1.976
X=-0.425 R=2.037

CASE NUMBER THREE

BETA=50.5 DEG
V0=0.810

X=-0.800 R=1.000
X=-0.765 R=1.007
X=-0.729 R=1.015
X=-0.694 R=1.025
X=-0.660 R=1.036
X=-0.632 R=1.045
X=-0.603 R=1.055
X=-0.575 R=1.066
X=-0.548 R=1.078
X=-0.525 R=1.090
X=-0.503 R=1.102
X=-0.482 R=1.115
X=-0.461 R=1.130
X=-0.451 R=1.138
X=-0.440 R=1.147
X=-0.430 R=1.155
X=-0.420 R=1.165
X=-0.412 R=1.173
X=-0.404 R=1.182
X=-0.396 R=1.191
X=-0.388 R=1.200
X=-0.384 R=1.206
X=-0.379 R=1.212
X=-0.375 R=1.219
X=-0.371 R=1.225
X=-0.366 R=1.234
X=-0.361 R=1.242
X=-0.357 R=1.257
X=-0.353 R=1.260
X=-0.349 R=1.268
X=-0.346 R=1.276
X=-0.343 R=1.284
X=-0.341 R=1.293
X=-0.339 R=1.300
X=-0.337 R=1.308
X=-0.335 R=1.316
X=-0.334 R=1.325
X=-0.333 R=1.331
X=-0.332 R=1.337
X=-0.331 R=1.344
X=-0.331 R=1.350
X=-0.327 R=1.443
X=-0.367 R=1.513
X=-0.399 R=1.611
X=-0.495 R=1.742
X=-0.561 R=1.830
X=-0.627 R=1.918

X=-0.000 R=1.600
X=-0.090 R=1.588
X=-0.101 R=1.654
X=-0.158 R=1.676
X=-0.175 R=1.734
X=-0.255 R=1.809
X=-0.322 R=1.897
X=-0.397 R=1.977
X=-0.469 R=2.059

```
C*************************************************************
C*                                                           **
C*                    APPENDIX I                             **
C*                                                           **
C*                FINITE ELEMENT METHOD                      **
C*                                                           **
C*    COMPUTATION OF THE ANGLE OF DEFLECTION AND THE         **
C*    COORDINATES OF THE FREE STREAMLINES FOR AN             **
C*          HEMISPHERICAL BUCKET                             **
C*                                                           **
C*************************************************************
C
      IMPLICIT REAL*8(A-H,O-Z)
C
      DIMENSION INO(288,6),JET(9,3),JABA(12,6),X(683),R(683)
     8,RR(65),XX(65),ELE(6,6),Z(683,60),B(683),ANGLE(45)
     8,V(80)
C
C VALUES FOR THE NUMBER OF ELEMENTS (NUMEL),BANDWIDTH (NBAN)
C NUMBER OF NODAL POINTS (NNODE),NODE AT LIP OF BUCKET (N2)
      NNODE=683
      NBAN=60
      N2=597
      NUMEL=288
      PI=3.1415926D0
      DK=1.0DO
C
C ASSIGN STARTING VALUES FOR DEFLECTION ANGLE (BETA) AND
C VELOCITY AT THE ENTRANCE OF THE NOZZLE (VO)
      BETA=0.8DO
      VO=0.85DO
      FACU=0.001DO
      FACL=0.02DO
C
C READ EQUIVALENCE OF NODAL POINTS
      READ(5,1) ( I,(INO(I,J),J=1,6),N=1,NUMEL)
    1 FORMAT(3(7I3))
C
C READ COORDINATES OF INTERIOR POINTS
      READ(5,2)(I,X(I),R(I),N=1,90)
    2 FORMAT(5(I3,F6.0,F5.0))
C
C READ X VALUES OF THE NODES OVER THE BUCKET
      READ(5,3) ( I,X(I),N=1,18)
    3 FORMAT(9(I3,F5.0))
C
C READ EQUIVALENCE OF NODES IN THE JET SECTION
      READ(5,4) ((JET(I,J),J=1,3),I=1,9)
    4 FORMAT(8(3I3))
C
C READ EQUIVALENCE OF NODES IN THEFLOATING GRID
      READ(5,5)((JABA(I,J),J=1,6),I=1,12)
    5 FORMAT(4(6I3))
C
C READ THE COORDINATES OF THE ASSUMED FREE SURFACE
      READ(5,6) (I,X(I),R(I),N=1,10)
    6 FORMAT(5(I3,F6.0,F5.0))
C
C LOCATE THE NODES OVER THE BUCKET
      RADIO=1.60D0
      DO 40 I=63,78
      J=INO(I,3)
   40 R(J)=DSQRT(RADIO**2-X(J)**2)
C
C LOCATE THE UPPER FREE SURFACE REALTIVE TO POINT N2
      DX=0.077D0
      DISP=0.0
      DO 10 I=55,59
      XD=61-I
      K=INO(I,1)
      X(K)=X(N2)-DX*XD
   10 R(K)=R(N2)-DTAN(BETA)*(X(K)-X(N2)+DISP)
```

```
C
C LOCATE THE POINTS CLOSE TO THE LIP
      ZR=R(647)-R(N2)
      X(617)=X(647)*0.25D0
      X(627)=X(647)*0.5D0
      X(637)=X(647)*0.75D0
      R(617)=R(N2)+ZR*0.25D0
      R(627)=R(N2)+ZR*0.50D0
      R(637)=R(N2)+ZR*0.75D0
      READ(5,6)(I,X(I),R(I),N=1,16)
      MAL=9
C
C STARTING POINT FOR ITERATIONS ON (BETA) AND (VC)
 10CC CONTINUE
      INDEX=0
C
C LOCATE THE REGION C OF THE LOWER FREE SURFACE
      TRES=0.05D0
      VETA=BETA+TRES
      DO 20 I=1,MAL
      I1=JET(I,1)
      I2=JET(I,2)
      I3=JET(I,3)
      IF(I.GE.8) GO TO 21
      R(I2)=DSQRT(R(I1)**2-VC*DCOS(VETA))
      X(I2)=X(I1)-DTAN(VETA)*(R(I1)-R(I2))
   21 X(I3)=(X(I1)+X(I2))*0.5D0
   20 R(I3)=(R(I1)+R(I2))*0.5D0
      X(591)=0.06D0
      R(591)=1.48D0
      X(606)=-0.16D0
      R(606)=1.48D0
      IF(MAL.EQ.9) X(618)=-0.33D0
      IF(MAL.EQ.9) R(618)=1.44D0
C
C STARTING POINT TO ITERATE THE FREE SURFACES
  100 CONTINUE
      INDEX=INDEX+1
C
C LOCATE THE INTERIOR POINTS IN THE FLOATING GRID
      DO 30 I=2,12
      I1=JABA(I,1)
      I2=JABA(I,2)
      I3=JABA(I,3)
      I4=JABA(I,4)
      I5=JABA(I,5)
      I6=JABA(I,6)
      X(I2)=X(I1)+0.15D0*(X(I4)-X(I1))
      X(I3)=X(I1)+0.5D0*(X(I4)-X(I1))
      R(I2)=R(I1)+0.15D0*(R(I4)-R(I1))
      R(I3)=R(I1)+0.50D0*(R(I4)-R(I1))
      X(I5)=0.5D0*(X(I6)+X(I2))
   30 R(I5)=0.5D0*(R(I6)+R(I2))
C
C LOCATE INTERMEDIATE POINTS IN ASSUMED LOWER FREE SURFACE
      DO 50 I=1,12
      K=JABA(I,1)
      XX(I)=X(K)
   50 RR(I)=R(K)
      CALL DRVFIT(2,12,RR,XX,4,45,RR,XX,ANGLE)
      DO 60 I=9,48
      K=INO(I,3)
      X(K)=XX(I-3)
   60 R(K)=RR(I-3)
      IF(MAL.NE.9) GO TO 28
      X(618)=-0.33D0
      R(618)=1.44D0
      X(628)=-0.36D0
      R(628)=1.52D0
      X(638)=-0.41D0
      R(638)=1.60D0
   28 CONTINUE
```

```
C
      RAD=57.2958D0
      ALFA3=DATAN((R(672)-R(647))/(X(647)-X(672)))*RAD
      WRITE(6,67) ALFA3,ALFA3
C CALCULATION OF THE DEFLECTION ANGLE ALFA
      ALFA1=DATAN((R(672)-R(667))/(X(667)-X(672)))*RAD
      ALFA2=DATAN((R(677)-R(657))/(X(657)-X(677)))*RAD
      GAMA1=DATAN((R(668)-R(648))/(X(648)-X(668)))*RAD
      GAMA2=DATAN((R(658)-R(638))/(X(638)-X(658)))*RAD
      WRITE(6,61) ALFA1,GAMA1
      WRITE(6,61) ALFA2,GAMA2
   61 FORMAT(5X,' UPPER FSL',F10.2,5X,' LOWER FSL',F10.2)
      GAMA3=DATAN((R(666)-R(658))/(X(658)-X(668)))*RAD
      GAMA4=DATAN((R(658)-R(648))/(X(648)-X(658)))*RAD
      WRITE(6,67) GAMA3,GAMA4
   67 FORMAT(2F20.2)
C
      WRITE(6,500) VO,BETA
  500 FORMAT(/,5X,' VO=',F10.4,5X,'BETA=',F10.4,/)
C
C ZERO OUT MATRICES (Z) AND (B)
      DO 42 L=1,NNODE
      DO 43 M=1,NBAN
   43 Z(L,M)=0.0D0
   42 B(L)  =0.0D0
C
C EVALUATE THE ELEMENTS OF MATRIX (Z)
      DO 44 K=1,NUMEL
      I1=INO(K,1)
      I2=INO(K,2)
      I3=INO(K,3)
      A1=X(I3)-X(I2)
      A2=X(I1)-X(I3)
      A3=X(I2)-X(I1)
      B1=R(I2)-R(I3)
      B2=R(I3)-R(I1)
      B3=R(I1)-R(I2)
      AREA=0.5*(A2*B1-A1*B2)
      S11=(A1*A1+B1*B1)/(AREA*60.0)
      S12=(A1*A2+B1*B2)/(AREA*60.0)
      S13=(A1*A3+B1*B3)/(AREA*60.0)
      S22=(A2*A2+B2*B2)/(AREA*60.0)
      S23=(A2*A3+B2*B3)/(AREA*60.0)
      S33=(A3*A3+B3*B3)/(AREA*60.0)
      ELE(1,1)=3.0*S11*(3.0*R(I1)+R(I2)+R(I3))
      ELE(1,2)=-S12*(2.0*R(I1)+2.0*R(I2)+R(I3))
      ELE(2,1)=ELE(1,2)
      ELE(1,3)=-S13*(2.0*R(I1)+R(I2)+2.0*R(I3))
      ELE(3,1)=ELE(1,3)
      ELE(1,4)=S11*(3.0*R(I1)-2.*R(I2)-R(I3))+S12*(14.0*R(
     8I1)+3.0*R(I2)+3.0*R(I3))
      ELE(4,1)=ELE(1,4)
      ELE(1,5)=S12*(3.*R(I1)-R(I2)-2.*R(I3))+S13*(3.0*R(I1
     8)-2.0*R(I2)-R(I3))
      ELE(5,1)=ELE(1,5)
      ELE(1,6)=S11*(3.0*R(I1)-R(I2)-2.0*R(I3))+S13*(14.0*R
     8(I1)+3.0*R(I2)+3.0*R(I3))
      ELE(6,1)=ELE(1,6)
      ELE(2,2)=3.0*S22*(R(I1)+3.0*R(I2)+R(I3))
      ELE(2,3)=-S23*(R(I1)+2.0*R(I2)+2.0*R(I3))
      ELE(3,2)=ELE(2,3)
      ELE(2,4)=S12*(3.0*R(I1)+14.0*R(I2)+3.0*R(I3))+S22*(-
     82.0*R(I1)+3.0*R(I2)-R(I3))
      ELE(4,2)=ELE(2,4)
      ELE(2,5)=S22*(-R(I1)+3.0*R(I2)-2.0*R(I3))+S23*(3.*R(
     8I1)+14.0*R(I2)+3.0*R(I3))
      ELE(5,2)=ELE(2,5)
      ELE(2,6)=S12*(-R(I1)+3.0*R(I2)-2.0*R(I3))+S23*(-2.0*
     8R(I1)+3.0*R(I2)-R(I3))
      ELE(6,2)=ELE(2,6)
      ELE(3,3)=3.*S33*(R(I1)+R(I2)+3.0*R(I3))
      ELE(3,4)=S13*(-R(I1)-2.0*R(I2)+3.0*R(I3))+S23*(-2.0*
```

```
     8R(I1)-R(I2)+3.0*R(I3))
       ELE(4,3)=ELE(3,4)
       ELE(3,5)=S23*(3.0*R(I1)+3.0*R(I2)+14.0*R(I3))+S33*(-
     8R(I1)-2.0*R(I2)+3.0*R(I3))
       ELE(5,3)=ELE(3,5)
       ELE(3,6)=S13*(3.0*R(I1)+3.0*R(I2)+14.0*R(I3))+S33*(-
     82.0*R(I1)-R(I2)+3.0*R(I3))
       ELE(6,3)=ELE(3,6)
       ELE(4,4)=8.0*(S11*(R(I1)+3.0*R(I2)+R(I3))+S12*(2.0*R
     8(I1)+2.0*R(I2)+R(I3))+S22*(3.*R(I1)+R(I2)+R(I3)))
       ELE(4,5)=8.0*S13*(R(I1)+3.0*R(I2)+R(I3))-4.*(S12*R(I
     81)+S22*R(I2)+S23*R(I3))
       ELE(5,4)=ELE(4,5)
       ELE(4,6)=8.0*S23*(3.0*R(I1)+R(I2)+R(I3))-4.*(S11*R(I
     81)+S12*R(I2)+S13*R(I3))
       ELE(6,4)=ELE(4,6)
       ELE(5,5)=8.0*(S22*(R(I1)+R(I2)+2.0*R(I3))+S23*(R(I1)
     8+2.0*R(I2)+2.0*R(I3)+S33*(R(I1)+3.*R(I2)+R(I3)))
       ELE(5,6)=8.0*S12*(R(I1)+R(I2)+3.0*R(I3))-4.0*(S13*R(
     8I1+S23*R(I2)+S33*R(I3))
       ELE(6,5)=ELE(5,6)
       ELE(6,6)=8.0*(S11*(R(I1)+R(I2)+2.0*R(I3))+S13*(2.0*R
     8(I1)+R(I2)+2.*R(I3))+S33*(3.*R(I1)+R(I2)+R(I3)))
C
C LOAD MATRIX (Z)
      DO 45 J=1,6
      II=INO(K,J)
      DO 46 L=1,6
      III=INO(K,L)
      IF(II.GT.III) GO TO 46
      NW=III-II+1
      IF(NW.GT.NBAN) NBAN=NW
      Z(II,NW)=Z(II,NW)+ELE(J,L)
   46 CONTINUE
   45 CONTINUE
   44 CONTINUE
C
C LOAD VECTOR (B) WITH BOUNDARY CONDITIONS
C
C AT THE INLET OF THE NOZZLE
      B(1)=-0.0
      B(2)=-R(3)*R(3)*VO/2.0
      B(3)=-R(3)*R(5)*VO/6.0
      B(4)=-(R(5)+R(3))*(R(5)-R(3))*VO/3.0
      B(5)=-R(5)*(R(7)-R(3))*VO/6.0
      B(6)=-(R(7)+R(5))*(R(7)-R(5))*VO/3.0
      B(7)=-R(7)*(R(9)-R(5))*VO/6.0
      B(8)=-(R(9)+R(7))*(R(9)-R(7))*VO/3.0
      B(9)=-R(9)*(R(9)-R(7))*VO/6.0
C
C AT THE EXIT OF THE JET (TAKE POTENTIAL=100.0)
      DO 70 I=668,672
      B(I)=10.0D12
   70 Z(I,1)=10.0D11
C
C SOLUTION OF THE POTENTIAL BY GAUSSIAN ELIMINATION
      MAL=2
      CALL BANDEC(Z,B,NNODE,NBAN,1,683,60,1)
C
C CALCULATIONS FOR THE VELOCITIES ALONG THE BOUNDARIES
      DO 110 I=1,79
      J1=INO(I,1)
      J3=INO(I,3)
      S=DSQRT((R(J1)-R(J3))**2+(X(J1)-X(J3))**2)
      V(I)=(B(J3)-B(J1))/S
      IF(I.GE.55) V(I)=-V(I)
      IF(I.GE.55) J3=J1
      WRITE(6,111) J3,X(J3),R(J3),V(I)
  111 FORMAT(5X,'NODE',I5,5X,' X=', F7.3,3X,'R=', F7.3,10X,'
     8 VELOC=',F7.3,/)
  110 CONTINUE
C
```

```
C VELOC. AT LIP OF NOZZLE (V1) AND LIP OF BUCKET (V2)
      V1=(B(194)-B(199))/0.0475D0
      V2=V(63)
      WRITE(6,112) V1,V2
  112 FORMAT(//,' VELOC. LIP1=',F10.4,5X,' VELOC. LIP2=',
     8F10.4,//)
C
C CORRECTION FOR THE UPPER AND LOWER FREE SURFACES
      WRITE(6,122)
C
C FOR THE LOWER FREE SURFACE
      DO 120 I=9,54
      AN=PI-BETA
      IF(I.LE.48) AN=ANGLE(I-4)
      K=IND(I,3)
      DELV=(V(I)**3-1.0)*FACL
      WRITE(6,121) K,DELV
      XX(I)=X(K)-DELV*DSIN(AN)
  120 RR(I)=R(K)+DELV*DCOS(AN)
C
C FOR THE UPPER FREE  SURFACE
      DO 130 I=55,62
      K=IND(I,1)
      DELV=(V(I)**3-1.0)*FACU
      WRITE(6,121) K,DELV
      XX(I)=X(K)+DELV*DSIN(AN)
  130 RR(I)=R(K)-DELV*DCOS(AN)
  122 FORMAT(/,' CORRECTIONS TO BE MADE AT EACH NODE ',/)
  121 FORMAT(5X,' NODE',I5,5X,' CORRECTION',F8.4)
      VC=VO-(V1-1.0)*VO
C
C RELOCATION OF THE NEW FREE SURFACE
      DO 140 I=9,62
      M=3
      IF(I.GE.55) M=1
      K=IND(I,M)
      X(K)=XX(I)
      R(K)=RR(I)
  140  CONTINUE
      DO 160 I=80,99
      I1=IND(I,1)
      I2=IND(I,2)
      I3=IND(I,3)
      IF(I.GE.94) I2=I3
      V3=(B(I2)-B(I1))/(X(I2)-X(I1))
      WRITE(6,161) I2,V3
  161 FORMAT(5X,'NODE=',I5,5X,'VELOC=',F9.3)
  160 CONTINUE
C
C EACH FIVE ITERATION CORRECT VO AND THE ANGLE BETA
      IF(INDEX.EQ.10) GO TO 101
      IF(INDEX.NE.5) GO TO 100
      FACU=0.015D0
      FACL=0.001D0
      GO TO 100
  101 CONTINUE
      FACU=0.001D0
      FACL=0.015D0
C
C CORRECTION OF THE ANGLE BETA
      DBE=0.03D0
      BETA=BETA+DBE
      DO 19 I=55,59
      XD=61-I
      K=IND(I,1)
      X(K)=X(N2)-DX*XD
   19  R(K)=R(N2)-DTAN(BETA)*(X(K)-X(N2)+DISP)
      ZR=R(647)-R(N2)
      X(617)=X(647)*0.25D0
      X(627)=X(647)*0.5D0
      X(637)=X(647)*0.75D0
      R(617)=R(N2)+ZR*0.25D0
```

```
      R(627)=R(N2)+ZR*0.50D0
      R(637)=R(N2)+ZR*0.75D0
      GO TO 1000
9999  CONTINUE
      STOP
      END
```

```
      SUBROUTINE BANDEC(A,F,NEQ,MAXB,NVEC,NROW,NBAN,NBEC)
      IMPLICIT REAL*8(A-H,O-Z)
      DIMENSION A(NROW,NBAN),F(NROW,NBEC)
      LOOP=NEQ-1
      DO 100 I=1,LOOP
      IF(DABS(A(I,1))-1.E-30 ) 1000,1000,10
   10 M=I+1
      N=MINO(I+MAXB-1,NEQ)
      DO 100 J=M,N
      L=J+2-M
      D=A(I,L)/A(I,1)
      DO 40 MM=1,NVEC
   40 F(J,MM)=F(J,MM)-D*F(I,MM)
      MM=MINO(MAXB-L+1,NEQ-J+1)
      DO 100 K=1,MM
      NN=L+K-1
  100 A(J,K)=A(J,K)-D*A(I,NN)
      DO 199 I=1,NVEC
  199 F(NEQ,I)=F(NEQ,I)/A(NEQ,1)
      DO 200 I=2,NEQ
      J=NEQ-I+1
      K=MINO(NEQ-J+1,MAXB)
      DO 200 MM=1,NVEC
      DO 190 L=2,K
      M=J+L-1
  190 F(J,MM)=F(J,MM)-A(J,L)*F(M,MM)
  200 F(J,MM)=F(J,MM)/A(J,1)
      RETURN
 1000  WRITE(6,1010) I
 1010  FORMAT(29H1  ZERO DIAGONAL ELEMENT ROW     I4)
      END
```

```
      SUBROUTINE  DRVFIT(MD,L,X,Y,M,N,U,V,ANGL)
C
      IMPLICIT REAL*8(A-H,O-Z)
      DIMENSION     X(L),Y(L),U(N),V(N)
     8,ANGL(N)
      EQUIVALENCE   (M1,B1),(M2,B2),(M3,B3),(M4,B4),
     1              (X2,P0),(Y2,Q0),(T2,C1)
      REAL*8        M1,M2,M3,M4
      EQUIVALENCE   (W2,Q2),(W3,Q3),(A1,P2),(B1,P3),
     1              (A2,DZ),(SW,R,Z)
C PRELIMINARY PROCESSING
   10 MDO=MD
      MDM1=MDO-1
      LO=L
      LM1=LO-1
      MO=M
      MM1=MO-1
      NO=N
      IF(MDO.LE.0)          GO TO 90
      IF(MDO.GE.3)          GO TO 90
      IF(LM1.LE.0)          GO TO 91
      IF(MM1.LE.0)          GO TO 92
      IF(NO.NE.LM1*MO+1)    GO TO 93
      GO TO (11,16), MDO
   11 I=2
      IF(X(1)-X(2))         12,95,14
   12 DO 13   I=3,LO
        IF(X(I-1)-X(I))     13,95,96
   13   CONTINUE
      GO TO 18
   14 DO 15   I=3,LO
        IF(X(I-1)-X(I))     96,95,15
   15   CONTINUE
      GO TO 18
   16 DO 17   I=2,LO
        IF(X(I-1).NE.X(I))  GO TO 17
        IF(Y(I-1).EQ.Y(I))  GO TO 97
   17   CONTINUE
   18 K=NO+MO
      I=LO+1
      DO 19   J=1,LO
        K=K-MO
        I=I-1
        U(K)=X(I)
   19   V(K)=Y(I)
      RM=MO
      RM=1.0/RM
C MAIN DO-LOOP
   20 K5=MO+1
      DO 80   I=1,LO
C ROUTINES TO PICK UP NECESSARY X AND Y VALUES AND
C          TO ESTIMATE THEM IF NECESSARY
        IF(I.GT.1)          GO TO 40
   30   X3=U(1)
        Y3=V(1)
        X4=U(MO+1)
        Y4=V(MO+1)
        A3=X4-X3
        B3=Y4-Y3
        IF(MDM1.EQ.0)       M3=B3/A3
        IF(LO.NE.2)         GO TO 41
        A4=A3
        B4=B3
   31   GO TO (33,32), MDO
   32   A2=A3+A3-A4
        A1=A2+A2-A3
   33   B2=B3+B3-B4
        B1=B2+B2-B3
        GO TO (51,56), MDO
   40   X2=X3
        Y2=Y3
        X3=X4
```

```
      Y3=Y4
      X4=X5
      Y4=Y5
      A1=A2
      B1=B2
      A2=A3
      B2=B3
      A3=A4
      B3=B4
      IF(I.GE.LM1)        GO TO 42
   41 K5=K5+M0
      X5=U(K5)
      Y5=V(K5)
      A4=X5-X4
      B4=Y5-Y4
      IF(MDM1.EQ.0)       M4=B4/A4
      GO TO 43
   42 IF(MDM1.NE.0)       A4=A3+A3-A2
      B4=B3+B3-B2
   43 IF(I.EQ.1)          GO TO 31
      GO TO (50,55), MDO
C NUMERICAL DIFFERENTIATION
   50 T2=T3
   51 W2=DABS(M4-M3)
      W3=DABS(M2-M1)
      SW=W2+W3
      IF(SW.NE.0.0)       GO TO 52
      W2=0.5
      W3=0.5
      SW=1.0
   52 T3=(W2*M2+W3*M3)/SW
      IF(I-1) 80,80,60
   55 COS2=COS3
      SIN2=SIN3
   56 W2=DABS(A3*B4-A4*B3)
      W3=DABS(A1*B2-A2*B1)
      IF(W2+W3.NE.0.0)  GO TO 57
      W2=DSQRT(A3*A3+B3*B3)
      W3=DSQRT(A2*A2+B2*B2)
   57 COS3=W2*A2+W3*A3
      SIN3=W2*B2+W3*B3
      R=COS3*COS3+SIN3*SIN3
      IF(R.EQ.0.0)        GO TO 58
      R=DSQRT(R)
      COS3=COS3/R
      SIN3=SIN3/R
   58 IF(I-1) 80,80,65
C DETERMINATION OF THE COEFFICIENTS
   60 Q2=(2.0*(M2-T2)+M2-T3)/A2
      Q3=(-M2-M2+T2+T3)/(A2*A2)
      GO TO 70
   65 R=DSQRT(A2*A2+B2*B2)
      P1=R*COS2
      P2=3.0*A2-R*(COS2+COS2+COS3)
      P3=A2-P1-P2
      Q1=R*SIN2
      Q2=3.0*B2-R*(SIN2+SIN2+SIN3)
      Q3=B2-Q1-Q2
      GO TO 75
C COMPUTATION OF THE POLYNOMIALS
   70 DZ=A2*RM
      Z=0.0
      DO 71  J=1,MM1
        K=K+1
        Z=Z+DZ
        U(K)=PO+Z
   71   V(K)=Q0+Z*(Q1+Z*(Q2+Z*Q3))
      GO TO 79
   75 Z=0.0
      DO 76  J=1,MM1
        K=K+1
        Z=Z+RM
```

```
            U(K)=P0+Z*(P1+Z*(P2+Z*P3))
   76       V(K)=Q0+Z*(Q1+Z*(Q2+Z*Q3))
   79     K=K+1
   80     CONTINUE
          DO 82 I=1,12
   82   ANGL(I)=0.0D0
          NM1=NO-1
          DO 81 K=12,NM1
   81   ANGL(K)=DATAN2((U(K+1)-U(K-1)),( V(K+1)-V(K-1)))
          RETURN
C ERROR EXIT
    90  WRITE (6,2090)
          GO TO 99
    91  WRITE (6,2091)
          GO TO 99
    92  WRITE (6,2092)
          GO TO 99
    93  WRITE (6,2093)
          GO TO 99
    95  WRITE (6,2095)
          GO TO 98
    96  WRITE (6,2096)
          GO TO 98
    97  WRITE (6,2097)
    98  WRITE (6,2098)    I,X(I),Y(I)
    99  WRITE (6,2099)    MDO,LO,MO,NO
          RETURN
C FORMAT STATEMENTS
  2090  FORMAT(1X/31H  ***    MD OUT OF PROPER RANGE./)
  2091  FORMAT(1X/22H  ***    L = 1 OR LESS./)
  2092  FORMAT(1X/22H  ***    M = 1 OR LESS./)
  2093  FORMAT(1X/25H  ***    IMPROPER N VALUE./)
  2095  FORMAT(1X/27H  ***    IDENTICAL X VALUES./)
  2096  FORMAT(1X/33H  ***    X VALUES OUT OF SEQUENCE./)
  2097  FORMAT(1X/33H  ***    IDENTICAL X AND Y VALUES./)
  2098  FORMAT(7H    I   =,I4,1CX,6HX(I) =,E12.3,
     1                      10X,6HY(I) =,E12.3)
  2099  FORMAT(7H   MD =,I4,8X,3HL =,I5,8X,
     1       3HM =,I5,8X,3HN =,I5/
     2       36H ERROR DETECTED IN ROUTINE    CRVFIT)
        END
```

CORNER NODAL POINTS AND THEIR COORDINATES

NODE	1	X=	-3.800	R=	0.0
NODE	3	X=	-3.800	R=	0.300
NODE	5	X=	-3.800	R=	0.600
NODE	7	X=	-3.800	R=	0.800
NODE	9	X=	-3.800	R=	1.000
NODE	19	X=	-3.300	R=	0.0
NODE	21	X=	-3.300	R=	0.300
NODE	23	X=	-3.300	R=	0.600
NODE	25	X=	-3.300	R=	0.800
NODE	27	X=	-3.300	R=	1.000
NODE	37	X=	-2.800	R=	0.0
NODE	39	X=	-2.800	R=	0.300
NODE	41	X=	-2.800	R=	0.600
NODE	43	X=	-2.800	R=	0.800
NODE	45	X=	-2.800	R=	1.000
NODE	55	X=	-2.300	R=	0.0
NODE	57	X=	-2.300	R=	0.300
NODE	59	X=	-2.300	R=	0.600
NODE	61	X=	-2.300	R=	0.800
NODE	63	X=	-2.300	R=	1.000
NODE	73	X=	-1.900	R=	0.0
NODE	75	X=	-1.900	R=	0.300
NODE	77	X=	-1.900	R=	0.600
NODE	79	X=	-1.900	R=	0.800
NODE	81	X=	-1.900	R=	1.000
NODE	91	X=	-1.500	R=	0.0
NODE	93	X=	-1.500	R=	0.300
NODE	95	X=	-1.500	R=	0.600
NODE	97	X=	-1.500	R=	0.800
NODE	99	X=	-1.500	R=	1.000
NODE	110	X=	-1.350	R=	1.000
NODE	111	X=	-1.200	R=	0.0
NODE	113	X=	-1.200	R=	0.300
NODE	115	X=	-1.200	R=	0.600
NODE	117	X=	-1.200	R=	0.800
NODE	119	X=	-1.200	R=	0.970
NODE	121	X=	-1.200	R=	1.000
NODE	125	X=	-1.150	R=	1.000
NODE	138	X=	-1.000	R=	0.0
NODE	140	X=	-1.000	R=	0.300
NODE	142	X=	-1.000	R=	0.600
NODE	144	X=	-1.000	R=	0.800
NODE	147	X=	-1.100	R=	0.970
NODE	150	X=	-1.100	R=	1.000
NODE	153	X=	-1.050	R=	1.000
NODE	156	X=	-1.000	R=	0.970
NODE	158	X=	-1.000	R=	1.000
NODE	162	X=	-0.950	R=	1.000
NODE	173	X=	-0.800	R=	0.0
NODE	175	X=	-0.800	R=	0.300
NODE	177	X=	-0.800	R=	0.600
NODE	179	X=	-0.800	R=	0.800
NODE	182	X=	-0.900	R=	0.955
NODE	184	X=	-0.800	R=	0.940
NODE	189	X=	-0.900	R=	1.000
NODE	190	X=	-0.850	R=	1.000
NODE	195	X=	-0.765	R=	1.005
NODE	200	X=	-0.800	R=	1.000
NODE	207	X=	-0.600	R=	0.0
NODE	209	X=	-0.600	R=	0.300
NODE	211	X=	-0.600	R=	0.600
NODE	213	X=	-0.620	R=	0.814

NODE	217	X=	-0.725	R=	0.952
NODE	219	X=	-0.651	R=	0.964
NODE	224	X=	-0.729	R=	1.011
NODE	226	X=	-0.694	R=	1.019
NODE	228	X=	-0.660	R=	1.028
NODE	230	X=	-0.630	R=	1.037
NODE	232	X=	-0.601	R=	1.046
NODE	244	X=	-0.400	R=	0.0
NODE	246	X=	-0.400	R=	0.300
NODE	248	X=	-0.400	R=	0.600
NODE	250	X=	-0.472	R=	0.835
NODE	253	X=	-0.587	R=	0.981
NODE	255	X=	-0.522	R=	0.999
NODE	261	X=	-0.572	R=	1.057
NODE	263	X=	-0.544	R=	1.069
NODE	265	X=	-0.521	R=	1.080
NODE	267	X=	-0.498	R=	1.092
NODE	279	X=	0.0	R=	0.0
NODE	281	X=	-0.100	R=	0.300
NODE	283	X=	-0.180	R=	0.600
NODE	285	X=	-0.318	R=	0.860
NODE	288	X=	-0.468	R=	1.020
NODE	290	X=	-0.414	R=	1.042
NODE	296	X=	-0.476	R=	1.105
NODE	298	X=	-0.455	R=	1.120
NODE	300	X=	-0.444	R=	1.128
NODE	302	X=	-0.433	R=	1.137
NODE	306	X=	-0.378	R=	1.059
NODE	316	X=	0.700	R=	0.0
NODE	318	X=	0.450	R=	0.270
NODE	320	X=	0.250	R=	0.450
NODE	322	X=	0.050	R=	0.620
NODE	324	X=	-0.181	R=	0.888
NODE	328	X=	-0.343	R=	1.076
NODE	334	X=	-0.422	R=	1.146
NODE	336	X=	-0.412	R=	1.156
NODE	338	X=	-0.404	R=	1.165
NODE	340	X=	-0.395	R=	1.174
NODE	357	X=	1.150	R=	0.0
NODE	361	X=	-0.387	R=	1.183
NODE	363	X=	-0.380	R=	1.193
NODE	366	X=	-0.314	R=	1.104
NODE	369	X=	1.600	R=	0.0
NODE	371	X=	1.350	R=	0.200
NODE	373	X=	1.400	R=	0.350
NODE	375	X=	0.740	R=	0.510
NODE	377	X=	0.500	R=	0.680
NODE	379	X=	0.250	R=	0.790
NODE	381	X=	-0.065	R=	0.991
NODE	383	X=	-0.286	R=	1.133
NODE	386	X=	-0.375	R=	1.200
NODE	388	X=	-0.371	R=	1.206
NODE	392	X=	-0.275	R=	1.155
NODE	408	X=	1.590	R=	0.179
NODE	412	X=	-0.367	R=	1.213
NODE	414	X=	-0.363	R=	1.220
NODE	420	X=	-0.032	R=	1.075
NODE	422	X=	0.300	R=	0.930
NODE	423	X=	1.550	R=	0.397
NODE	424	X=	1.470	R=	0.632
NODE	426	X=	1.150	R=	0.720
NODE	428	X=	0.800	R=	0.810
NODE	430	X=	0.500	R=	0.890
NODE	432	X=	-0.264	R=	1.177
NODE	434	X=	-0.358	R=	1.229
NODE	436	X=	-0.354	R=	1.238
NODE	455	X=	-0.256	R=	1.205
NODE	456	X=	-0.023	R=	1.179
NODE	460	X=	-0.350	R=	1.248

NODE	465	X=	-0.346	R=	1.257
NODE	467	X=	-0.249	R=	1.233
NODE	469	X=	0.300	R=	1.100
NODE	471	X=	0.550	R=	1.100
NODE	473	X=	0.820	R=	1.100
NODE	475	X=	1.160	R=	1.102
NODE	477	X=	1.390	R=	0.792
NODE	478	X=	1.280	R=	0.960
NODE	483	X=	1.030	R=	1.224
NODE	494	X=	-0.250	R=	1.259
NODE	499	X=	-0.343	R=	1.265
NODE	501	X=	-0.340	R=	1.274
NODE	503	X=	0.875	R=	1.340
NODE	505	X=	-0.338	R=	1.282
NODE	507	X=	-0.336	R=	1.291
NODE	512	X=	-0.053	R=	1.271
NODE	514	X=	0.230	R=	1.250
NODE	516	X=	0.480	R=	1.300
NODE	518	X=	0.725	R=	1.426
NODE	522	X=	-0.251	R=	1.285
NODE	525	X=	-0.335	R=	1.299
NODE	529	X=	-0.333	R=	1.307
NODE	531	X=	-0.254	R=	1.310
NODE	541	X=	0.590	R=	1.487
NODE	543	X=	0.460	R=	1.532
NODE	544	X=	0.350	R=	1.561
NODE	546	X=	0.160	R=	1.400
NODE	548	X=	-0.086	R=	1.362
NODE	553	X=	-0.332	R=	1.316
NODE	556	X=	-0.231	R=	1.324
NODE	558	X=	-0.257	R=	1.335
NODE	561	X=	0.240	R=	1.582
NODE	570	X=	-0.264	R=	1.352
NODE	573	X=	-0.330	R=	1.330
NODE	576	X=	-0.330	R=	1.337
NODE	579	X=	-0.329	R=	1.343
NODE	585	X=	-0.329	R=	1.350
NODE	587	X=	-0.271	R=	1.370
NODE	589	X=	-0.135	R=	1.415
NODE	591	X=	0.000	R=	1.480
NODE	593	X=	0.155	R=	1.592
NODE	595	X=	0.070	R=	1.598
NODE	597	X=	0.0	R=	1.600
NODE	599	X=	0.025	R=	1.600
NODE	606	X=	-0.160	R=	1.480
NODE	608	X=	-0.212	R=	1.414
NODE	617	X=	-0.038	R=	1.640
NODE	618	X=	-0.330	R=	1.440
NODE	620	X=	-0.177	R=	1.591
NODE	627	X=	-0.077	R=	1.679
NODE	628	X=	-0.360	R=	1.520
NODE	632	X=	-0.249	R=	1.675
NODE	635	X=	-0.091	R=	1.593
NODE	637	X=	-0.116	R=	1.719
NODE	638	X=	-0.410	R=	1.600
NODE	642	X=	-0.322	R=	1.758
NODE	644	X=	-0.166	R=	1.675
NODE	647	X=	-0.154	R=	1.759
NODE	648	X=	-0.481	R=	1.765
NODE	654	X=	-0.395	R=	1.841
NODE	657	X=	-0.231	R=	1.838
NODE	658	X=	-0.551	R=	1.851
NODE	662	X=	-0.468	R=	1.923
NODE	667	X=	-0.308	R=	1.917
NODE	668	X=	-0.621	R=	1.936
NODE	670	X=	-0.542	R=	2.006
NODE	672	X=	-0.462	R=	2.076
NODE	677	X=	-0.385	R=	1.996

LIST OF REFERENCES

1. Sarpkaya, T., Deflection of Jets, II, Symmetrically Placed U-Shaped Obstacle, Studies in Engineering, 35, State University of Iowa, 1953.

2. Tinney, E. R., Barnes, W. E., Rechard, O. W. and Ingram, G. R., "Free-streamline Theory for Segmental Jet Deflectors," J. Hydraul. Div., ASCE, V. 87, No. HY5, p. 135-145, 1961.

3. Chang, H. Y. and Conly, J. F., "Potential Flow of Segmental Jet Deflectors," J. Fluid Mech., V. 46, pt. 3, p. 465-475, 1971.

4. Milne-Thomson, L. M., Theoretical Hydrodynamics, Macmillan, 1968.

5. Schieldrop, E. B., "Two-Dimensional Fluid Motion Bounded by Straight and Curved Fixed Walls and Free Surfaces," Skrifter Utgitt av Det Norske Videnskaps-Akademi I Oslo Matem. Naturv. Klasse. No. 6, 1928.

6. Cockcroft, J. D., "The Effect of Curved Boundaries on the Distribution of Electrical Stress Round Conductors," J. Inst. Electr. Eng., V. 66, p. 385-409, 1928.

7. Carrier, G. F., Krook, M. and Pearson, C. E., Functions of a Complex Variable, McGraw-Hill, 1966.

8. Larock, B. E. and Street, R. L., "A Riemann-Hilbert Problem for Non-Linear, Fully Cavitating Flow," J. Ship Res., V. 9, p. 170-177, 1965.

9. Larock, B. E., "Jets from Two-Dimensional Symmetric Nozzles of Arbitrary Shape," J. Fluid Mech., V. 37, pt. 3, p. 479-489, 1969.

10. Brillouin, M. M., "Les Surfaces de Glissement D'Helmholtz et la Resistance des Fluides," Ann. Chimie et Phys., V. 23, No. 8, p. 145-230, 1911.

11. Villat, H., "Sur la Resistance des Fluids," Ann. Sci. Ec. Norm. Sup. Paris, V. 28, p. 203-240, 1911.

12. Levi-Civita, T., "Scie e Leggi di Resistenza," R. Circ. Mat. Palermo, V. 23, p. 1-37, 1907.

13. Robertson, J. M., Hydrodynamics in Theory and Application, Prentice-Hall, 1965.

14. Birkhoff, G. and Zarantonello, E. H., Jets Wakes, and Cavities, Academic Press, 1957.

15. Cisotti, V., "Vene Fluenti," Circ. Mat., Palermo, V. 25, p. 145-179, 1908.

16. Wu, T. Y., "A Free Streamline Theory for Two-Dimensional Fully Cavitated Hydrofoils," J. Math. and Phys., V. 35, pt. 3, p. 236-265, Oct. 1956.

17. Cisotti, V., "Sulla Biforcazione di una Vena Liquida," Rend. Acad. Naz. Linc., Rome, V. 20, No. 5, p. 494-502, 1911.

18. Cheng, H. K. and Rott, N., "Generalization of the Inversion Formula of Thin Airfoil Theory," J. Rat. Mech. Anal., V. 3, p. 357-382, 1954.

19. Song, C. S., A Quasi-Linear and Linear Theory for Non-Separated and Separated Two-Dimensional, Incompressible, Irrotational Flow About Lifting Bodies, University of Minnesota, Minneapolis S.A.F. Hydraulic Lab. Tech. Paper, B43, 1963.

20. Hartree, D. R., Numerical Analysis, Clarendon Press, 1958.

21. Schaach, W. V., "Umlemkung eines freien Flussigkeitsstrahles an einer ebenen Platte," Ing. Arch., V. 5, p. 245-265, 1934.

22. Trefftz, E., "Uber die Kontraktion Kreisformiger Flussigkeitz-strahlen," Zeit. fuer Ang. Math. und Phys., V. 64, p. 34, 1917.

23. Southwell, R. and Vaisey, G., "Relaxation Methods Applied to Engineering Problems. XII. Fluid Motions Characterized by Free Streamlines," Phil. Trans. Royal Soc. of London, Ser. A, V. 240, p. 117-161, 1948.

24. Rouse, H. and Abul-Fetouh, A., "Characteristics of Irrotational Flow Through Axially Symmetric Orifices," J. Applied Mech., V. 17, No. 4, p. 421-426, 1950.

25. Garabedian, P., "Calculation of Axially Symmetric Cavities and Jets," Pacif. J. of Math., V. 6, p. 611-684, 1956.

26. Hunt, B. W., "Numerical Solution of an Integral Equation for Flow From a Circular Orifice," J. Fluid Mech., V. 31, pt. 2, p. 361-377, 1968.

27. Schnurr, N. M., Williamson, J. W. and Tatom, J. W., "An Analytical Investigation of the Impingement of Jets on Curved Deflectors," J. AIAA., V. 10, No. 11, p. 1430-1435, Nov. 1972.

28. Jeppson, R. W., "Inverse Formulation and Finite Difference Solution for Flow from a Circular Orifice," J. Fluid Mech., V. 40, pt. 1, p. 215-223, 1970.

29. Jeppson, R. W., "Numerical Solution to Free-Surface Axisymmetric Flows," J. Eng. Mech. Div., ASCE, V. 95, No. EM1, p. 1-20, 1969.

30. Zienkiewicz, O. C. and Cheung, Y. K., "Finite Elements in the Solution of Field Problems," The Engineer, V. 24, p. 507-510, Sept. 1965.

31. Norrie, D. A. and de Vries, G., Application of Finite Elements Methods in Fluid Dynamics, Num. Meth. in Fluid Dyn. Egard Lect. Series, No. 48, (Ed. by J. J. Smolderen), Harford House, London, p. 12-1/12-39, May 1972.

32. Chan, S. T. K. and Larock, B. E., "Fluid Flows from Axisymmetric Orifices and Valves," J. Hydraul. Div., ASCE, V. 99, No. HY1, p. 81-95, 1973.

33. Felippa, C. A., Refined Finite Element Analysis of Linear and Non-Linear Two-Dimensional Structures, Structural Engrg. Lab., Univ. of California, Berkeley, Report No. SESM 66-22, Oct. 1966.

34. Steffen, F. W., McArdle, J. G. and Coats, J. W., Performance Characteristics of Hemispherical Target-Type Thrust Reversers, N.A.C.A., RM. E55E18, June 1955.

35. Povolny, J. H., Steffen, F. W. and McArdle, J. G., Summary of Scale-Model Thrust-Reverser Investigation, N.A.C.A., Rep. 1314, Dec. 1955.

INITIAL DISTRIBUTION LIST

		No. Copies
1.	Defense Documentation Center Cameron Station Alexandria, Virginia 22314	2
2.	Library, Code 0212 Naval Postgraduate School Monterey, California 93940	2
3.	Professor T. Sarpkaya Department of Mechanical Engineering Naval Postgraduate School Monterey, California 93940	5
4.	Department of Mechanical Engineering Naval Postgraduate School Monterey, California 93940	2
5.	Gerardo HIRIART Le Bert 38 Marion Avenue Salinas, California 93901	5
6.	Director de Ingenieria de la Armada Correo Naval Valparaiso - Chile	2

REPORT DOCUMENTATION PAGE

READ INSTRUCTIONS BEFORE COMPLETING FORM

1. REPORT NUMBER

2. GOVT ACCESSION NO.

3. RECIPIENT'S CATALOG NUMBER

4. TITLE (and Subtitle)
A Theoretical Analysis of Jet Deflection From Plane and Axisymmetric Curved Obstacles

5. TYPE OF REPORT & PERIOD COVERED
Ph.D. Thesis; December 1973

6. PERFORMING ORG. REPORT NUMBER

7. AUTHOR(s)
Gerardo HIRIART Le-Bert

8. CONTRACT OR GRANT NUMBER(s)

9. PERFORMING ORGANIZATION NAME AND ADDRESS
Naval Postgraduate School
Monterey, California 93940

10. PROGRAM ELEMENT, PROJECT, TASK AREA & WORK UNIT NUMBERS

11. CONTROLLING OFFICE NAME AND ADDRESS
Naval Postgraduate School
Monterey, California 93940

12. REPORT DATE
December 1973

13. NUMBER OF PAGES
129

14. MONITORING AGENCY NAME & ADDRESS(if different from Controlling Office)
Naval Postgraduate School
Monterey, California 93940

15. SECURITY CLASS. (of this report)
Unclassified

15a. DECLASSIFICATION/DOWNGRADING SCHEDULE

16. DISTRIBUTION STATEMENT (of this Report)
Approved for public release; distribution unlimited.

17. DISTRIBUTION STATEMENT (of the abstract entered in Block 20, if different from Report)

18. SUPPLEMENTARY NOTES

19. KEY WORDS (Continue on reverse side if necessary and identify by block number)
Jets
Curved Obstacles
Jet Deflection
Thrust Reversers
Potential Flow with Free Surfaces
Finite element analysis of axisymmetric jet deflection

20. ABSTRACT (Continue on reverse side if necessary and identify by block number)
A class of analytical and numerical solutions to the problem of inviscid-jet deflection from plane and axisymmetric concave surfaces are presented. The methods of solution for the two-dimensional cases included a novel method developed in the present investigation, as well as those due to Levi-Civita and Riemann and Hilbert. These methods have provided indirect solutions for the shape of the curved solid boundary in terms of

(20. continued)

a given jet-departure and jet-deflection angle. The axisymmetric cases, namely, the deflection of axisymmetric jets from hemispherical thrust reversers are solved directly through the use of the finite element method and a novel iteration scheme. The real-fluid effects on the jet deflection are estimated by comparing the results with those obtained experimentally.

The analytical and numerical methods developed or used herein are sufficiently general to yield direct and indirect solutions for more general nozzle and curved-reverser combinations of special interest to thrust reversal on aircraft engines.

Thesis
H5775 Hiriart Le-Bert
c.1 A theoretical analysis of jet deflection from plane and axisymmetric curved obstacles.